Energy & Environmental Science

Accepted Manuscript

ROYAL SOCIETY OF CHEMISTRY

www.rsc.org/ees

Energy & Environmental Science

RSCPublishing

PERSPECTIVE

Nonaqueous Redox-Flow Batteries: Organic Solvents, Supporting Electrolytes, and Redox Pairs

Cite this: DOI: 10.1039/xoxxoooooox

Ke Gong,[a] Qianrong Fang,[a] Shuang Gu,[a,*] Sam Fong Yau Li,[b] and Yushan Yan[a,*]

Received ooth January 2014,
Accepted ooth January 2014

DOI: 10.1039/xoxxoooooox

www.rsc.org/

As a family member of redox-flow batteries (RFBs), nonaqueous RFBs can offer wide working temperature, high cell voltage, and potentially high energy density. These key features make nonaqueous RFBs an important complement of aqueous RFBs, broadening the spectrum of RFB applications. The development of nonaqueous RFBs is still at its early research stage and great challenges remain to be addressed before successful for practical applications. As such, it is essential to understand the major components in order to advance the nonaqueous RFB technology. In this perspective, three key major components of nonaqueous RFBs: organic solvent, supporting electrolyte, and redox pairs are selectively focused and discussed, with the emphases on providing an overview for those components and on highlighting the relationship between structure and property. Urgent challenges are also discussed. To advance nonaqueous RFBs, the understanding of both components and systems is critically needed and it calls for inter-disciplinary collaborations across expertise including electrochemistry, organic chemistry, physical chemistry, cell design, and system engineering. In order to demonstrate key features of nonaqueous RFBs, herein we also present an example of designing a 4.5 V ultrahigh-voltage nonaqueous RFB by combining BP/BP•$^{-}$ redox pair and ONF•$^{+}$/OFN redox pair.

1. Introduction

The first redox-flow battery (RFB) was invented by Thaller in 1974.[1] Unlike traditional rechargeable batteries, the energy-carrying redox pairs of RFBs are liberated from the solid electrodes into liquid electrolytes. The decoupling between energy storage and power delivery provides unprecedented design flexibility and scalability.[2, 3] Significant efforts and progresses have been made in developing efficient and economical RFB systems in the last two decades,[4-22] mostly driven by the needs for addressing the intermittency of the fast growing renewable energy like wind and solar.

The majority of RFBs are based on aqueous solutions as electrolytes, and aqueous RFBs have demonstrated high cell performance, low battery cost, and excellent system reliability. Similar to aqueous solutions, organic solvents can also be used to prepare electrolytes for RFBs. Since the first concept of nonaqueous RFB was proposed by Singh in 1984,[23] many types of nonaqueous RFBs have been invented and studied, which clearly validate the feasibility of using organic solvents for RFBs. Milestone examples for nonaqueous RFBs constructed with metal-based redox systems includes: $Ru(acac)_3$, $Ru(bpy)_3$, or $Fe(bpy)_3$ by Matuda et al. in 1988;[24] a series of U-ligand based redox pairs by Yamamura et al. in 2002;[25] $V(acac)_3$ by Thomphson et al. in 2009[26] and $Mn(acac)_3$ in 2011;[27] $Cr(acac)_3$ by Sleightholme et al. in 2010;[28] $Ni(bpy)_3$ by K.J. Kim and Y.K. Kim et al. in 2011;[29] $Co(acacen)_3$ by Li et al. in 2012;[30] polyoxometalate by Anderson et al. in 2013[31] and $V(mnt)_3$ in 2014.[32]

Regarding nonaqueous RFBs that are constructed by metal-free redox systems (or all-organic nonaqueous RFB), Chakrabarti et al., reported rubrene based nonaqueous RFB in 2007;[33] Liu et al. reported 2,2,6,6,-tetramethyl-1-1piperidinyloxyl (TEMPO•, "•" stands for radical, hereinafter) and N-methylphthalimide (NMI) based nonaqueous RFB in 2011;[34] Jansen et al. introduced 2,5-di-tert-butyl-1,4-bis(2-methoxyethoxy)benzene (DBBB) and a variety of quinoxalines based nonaqueous RFB in 2012;[16] and Wang, Xu, and co-workers introduced anthraquinone redox system into nonaqueous RFB in 2012.[18]

In addition to the conventional all-soluble nonaqueous RFBs, the territory of nonaqueous RFB is also extended by utilizing a solid metal (e.g., Li) as negative electrode,[18, 35] or deploying a suspension electrode-electrolyte.[36, 37] Furthermore, the combination of nonaqueous electrolyte and aqueous one opens up an important research direction, exemplified by the recent breakthroughs.[14, 15, 38-49]

Compared with aqueous RFBs, nonaqueous RFBs can offer wide working temperature, high cell voltage, and potentially high energy density, thanks to the nature of organic solvents. As a family member of RFBs, nonaqueous RFBs, especially those with the ability to work at low temperatures, are an important complement of aqueous RFBs, broadening the spectrum of RFB applications.

In spite of increasing interest received worldwide, the development of nonaqueous RFBs is still at its early research stage and great challenges remain to be addressed before the success for practical applications. As such, it is essential to

understand the major components in order for us to advance nonaqueous RFB technologies. Cell types and structures of current nonaqueous RFBs have been summarized in an excellent review paper by Wang et al. in 2013.[12] Membranes as well as cell performances of nonaqueous RFBs have been discussed in a comprehensive review paper by Moon et al., in the same year 2013.[21] A comprehensive cost analysis comparing nonaqueous and aqueous RFBs has been presented by Darling, Gallagher, and their colleagues in their outstanding paper published in 2014.[50] Note that lithium-ion batteries are also a competing nonaqueous battery, and recent advances have been achieved and summarized by a recent book.[51] In this perspective, key features of nonaqueous RFBs are highlighted; and three key components of nonaqueous RFBs: organic solvent, supporting electrolytes, and redox pairs, are selectively focused and discussed, with the emphases on providing an overview for those components and on highlighting the relationship between structure and property. In addition, two key urgent challenges are also discussed. At the end we also present an example of designing a 4.5 V ultrahigh-voltage nonaqueous RFB by combining BP/BP•$^{-}$ redox pair and ONF•$^{+}$/OFN redox pair.

2. Features of nonaqueous RFBs

2.1. Wide working temperature

The air temperature of about a half of the Earth's land can drop below 0 °C in winters (e.g., January at the northern hemisphere, 1959−1997, **Figure 1**, from Global Climate Animations), and the lowest temperature recorded on the Earth – which was measured by the Russian Vostok Station on July 21, 1983 – was −89.2°C in Antarctica. Low temperature could pose a significant challenge to the traditional aqueous RFBs since water solvent-based electrolytes tend to freeze at sufficiently low temperatures. By contrast, many organic solvents have low freezing points and appropriate boiling points. For example, tetrahydrofuran (THF) and 1-propanol have a freezing point of −108 °C and −126 °C, respectively, and these solvents based electrolytes would never freeze spontaneously on the Earth even in the coldest areas. There are many other solvents with different freezing points and distinctive properties available for nonaqueous RFBs (**Table 1**).

2.2. High cell voltage

Water solvent has an electrochemical window (ECW**)** of 1.23 V (25 °C, 100 kPa) and such a narrow ECW fundamentally limits the cell voltage of aqueous RFBs and the choice of RFB chemistries. By contrast, many organic solvents can offer an ECW of over 5 V. Examples include acetonitrile (AN) and γ-valerolactone (GVL) which have an ECW of 6.1 V and 8.2 V, respectively (**Table 2**). The wide ECW allows redox pairs with very low redox potential for negative electrolyte and very high redox potentials for positive electrolyte at the same time, offering high cell voltages without the concern of solvent breakdown. For example, in AN solvent with 0.5 M Et_4NBF_4 as supporting electrolyte, the $V(acac)_3$ based nonaqueous RFB offers a formal cell voltage of 2.2 V,[26] and the $Cr(acac)_3$ based counterpart does a formal cell voltage of 3.4 V.[28] Since higher cell voltage leads proportionally to higher energy density and power density, nonaqueous RFBs in principle have the possibility to achieve high specific energy and/or high power density.

2.3. Potentially high energy density

The solubility of redox compounds in aqueous electrolytes is generally low (around 1 M), except for some special redox pairs such as polybromide and polyiodide. The low solubility, together with low cell voltage, is the key cause for the generally low specific energy for aqueous RFBs, compared with other rechargeable battery technologies. The increase of solubility of redox compounds in aqueous electrolytes has been recognized as a major hurdle, largely because the water solvent substantially dictates the solubility. By contrast, there are many types of organic solvents available to work with redox compounds. Every solvent has a distinctive ability to dissolve certain compounds, and hence it is possible to find some solvents with sufficiently high solubility to construct RFBs with high energy density.

3. Organic solvents

3.1. Freezing/boiling temperatures

Dissolving solute usually depresses the freezing point and elevates the boiling point of a solvent, but the suppression and elevation are generally limited. For example, water and ethanol have a cryoscopic constant ($\boldsymbol{K_f}$) of 1.86 and 1.99 K $kg_{solvent}^{-1}$ mol_{solute}, respectively; and they have an ebullioscopic constant ($\boldsymbol{K_b}$) of 0.51 and 1.19 K $kg_{solvent}^{-1}$ mol_{solute}, respectively (data from www.vaxasoftware.com). These small cryoscopic constants (and ebullioscopic constants) indicate that the unit concentration of a solute can supress (and elevate) only up to a few degrees for the freezing point (and boiling point) of the solvent, by the following equations (**Eq.s 1** and **2**):

$$\Delta T_f = K_f \cdot m \cdot n \qquad \textbf{Eq. 1}$$

where ΔT_f, K_f, m, n are freezing point suppression, cryoscopic constant, mass molar concentration, and van't Hoff factor (the number of particles the solute splits into or forms when dissolved), respectively.

$$\Delta T_b = K_b \cdot m \cdot n \qquad \textbf{Eq. 2}$$

where ΔT_b and K_b are the boiling point elevation and ebullioscopic constant, respectively; m, n are the same as in **Eq. 1**.

Organic solvents can offer very wide working temperatures, and there are a large number of solvents that have been used for electrochemical applications. The comprehensive book entitled "*Electrochemistry in Nonaqueous Solutions*" written by Izutsu is a must read for choosing nonaqueous solvents and understanding nonaqueous electrochemistry.[52] **Table 1** lists some common organic solvents as possible choices for nonaqueous RFBs are included. Only organic solvents with a freezing point of −20 °C or below and a boiling point of 40 °C or above are included. Note that 40 °C is the highest average temperature in summer on the Earth surface (e.g., July at the northern hemisphere, 1959−1997). There are also other considerations (saturated vapour pressure, toxicity, and electrochemical window) for inclusion in **Table 1**.

3.2. Electrochemical window

Under standard conditions (25 °C, 100 kPa), water solvent has well-defined ECWs with reversible reduction potential of water (i.e., hydrogen evolution) of −0.83 and 0 V vs. SHE at pH = 14 and 0, respectively; and reversible oxidation potential of water

(i.e., oxygen evolution) of 0.40 and 1.23 V vs. SHE at pH = 14 and 0, respectively. However, the reversible reduction and oxidation potentials of organic solvents are neither practically useful nor easily obtainable. Instead, empirical methods are often used to define the ECWs of organic solvents and different criteria have been used for the evaluation of limiting reduction potentials (E_{red}) and limiting oxidation potentials (E_{oxi}). The E_{red} and E_{oxi} data of some organic solvents are from Ue's excellent work with a threshold current density of 1 mA cm^{-2} on glassy carbon electrode at 25 °C (0.65 M Et_4NFB_4 as supporting electrolyte and 5 mV s^{-1} as scan rate, **Table 1**). Note that caution is needed to compare the ECWs among organic solvents because different criteria and different test conditions (such as electrode materials, supporting electrolyte, and cyclic voltammetry method) may substantially impact both E_{red} and E_{oxi}. Regardless of evaluation methods used, the oxidation is generally much higher for those organic solvents (2.9−5.4 V vs. SHE) than for water solvent (0.40−1.23 V vs. SHE depending on pH); at the same time the reduction potential is lower for the former than for the latter (**Table 1**). Electrochemically, organic solvents are much more stable than water solvent.

3.3. Viscosity

The viscosity of organic solvents plays an important role in determining the ionic conductivity for organic solutions that contain supporting electrolytes. In general, lower solvent viscosity leads to higher ionic conductivity for a given supporting ion, governed by the Stokes' law (**Eq. 3**)

$$\Lambda_m = (z^2 \cdot F^2/\pi \cdot N_A)/(k \cdot \mu \cdot r) \quad \text{Eq. 3}$$

where Λ_m is limiting molar conductivity, z is charge number, F is Faraday constant, π is the mathematical constant, N_A is Avogadro constant, k is Stokes constant (k = 4 stands for slip friction, and k = 6 does for stick friction), μ is viscosity of solvent, and r is ionic radius.

Since the ionic conductivity of electrolytes controls the cell resistance and thus the voltage efficiency of RFBs, the viscosity of the organic solvent deserves careful consideration in designing nonaqueous RFBs. **Table 2** shows the limiting ionic conductivity of some common supporting ions in four typical organic solvents with distinctive viscosities. Clearly, the lower viscosity, the higher ionic conductivity. In particular, AN and dichloromethane (DCM) solvents have a very low viscosity of 0.34 and 0.39 mPa·s, respectively, and they usually offer very high limiting molar conductivity for supporting ions. In fact, AN has been the most often used organic solvent for nonaqueous electrochemistry studies and nonaqueous RFB applications as well. Water solvent is not an exception for the Stokes' law. Water has a moderate viscosity of 0.89 mPa·s, and thus water offers moderate limiting molar conductivity for supporting ions. In addition to the impact on limiting molar conductivity of supporting ions, the viscosity of organic solvents determines the pumping cost: higher viscosity brings higher pumping cost at a given flow rate of electrolyte.

3.4. Relative permittivity

Another very important parameter to consider for an organic solvent is its relative permittivity (ε_r, or dielectric constant). The relative permittivity can impact not only the solubility of supporting electrolytes but also the dissociation constant of the supporting electrolyte when dissolved. Both solubility and dissociation constant can significantly influence the practical ionic conductivity for the organic solvent with supporting electrolyte.

The general trend is that higher relative permittivity of an organic solvent leads to higher solubility for supporting electrolytes (**Table 3**). Apparently, organic solvents with large relative permittivity (e.g., ε_r: 36.7 and 35.9 for AN and DMF, respectively) have higher solubility for supporting electrolytes than those with small relative permittivity (e.g., ε_r: 7.58 and 7.20 for THF and DME, respectively). PC, BC, and GVL have very high relative permittivity (ε_r: 64.9, 53.0, and 42.0, respectively) and thus they are expected to offer even higher solubility for supporting electrolytes. By contrast, the organic solvents with very low relative permittivity such as hexane and toluene (ε_r: 1.88 and 2.38, respectively) have very limited solubility for common supporting electrolytes. Even though they have very low viscosity (ε_r: 0.29 and 0.55 mPa·s, respectively), their solutions have very low ionic conductivity, limiting their use as nonaqueous solvent for electrochemical applications. In general, supporting electrolytes have lower solubility in organic solvents than in water due to water's much higher relative permittivity (78.39). For example, NaCl has a solubility of 5.4 M in water, which is substantially higher than those of organic supporting electrolytes in organic solvents. Note that other parameters (such as dipole moment, and acidity & basicity) also have substantial impacts on solubility and caution is needed in predicting solubility in organic solvents.

Besides impacting the solubility of supporting electrolytes, the relative permittivity also dictates the dissociation constant (K_d) for supporting electrolytes. The relationship between K_d and ε_r can be described by the Denison-Ramsey equation (**Eq. 4**)[53]

$$\ln(K_d) = q_e^2/(\varepsilon_0 \cdot \varepsilon_r \cdot L \cdot k_B \cdot T) \quad \text{Eq. 4}$$

where, K_d is dissociation constant; q_e is elementary charge; ε_0 and ε_r are the permittivity of vacuum and relative permittivity of solvent, respectively; L is the distance of closest approach of the two ions of a dissolving salt; k_B is Boltzmann's constant, and T is absolute temperature. Note that the association constant, K_a, was used in the original equation and the dissociation constant, K_d, is used here ($K_d = 1/K_a$).

Note that L could be far larger than the sum of radii of two ions of a salt, e.g., an L value of 16.4 nm was observed for Bu_4NPF_6 in fitting a group of organic solvents in a recent work[54] and such a large L value is about 25 times that the sum of radii of Bu_4N^+ and PF_6^- (**Table 2**). The physical meaning of L has not been well understood so far.

Basically, the Denison-Ramsey equation shows the linear relationship between the natural logarithms of K_d of a given supporting electrolyte and the reciprocal of relative permittivity of solvent. Larger relative permittivity of organic solvent leads to larger dissociation constant for a given supporting electrolyte. For example, the dissociation constant of Bu_4NClO_4 drastically increases from $10^{-5.57}$ in THF (ε_r: 7.58) to $10^{-0.45}$ in PC (ε_r: 64.9) (**Table 4**). The dissociation constant of those supporting electrolytes in organic solvents is significantly lower than in water. For example, NaCl has a large dissociation constant of $10^{0.74}$ in water.[55] Note that organic supporting electrolytes also have a similarly large dissociation constant (e.g., K_d: $10^{0.78}$ for Bu_4NI)[56] in water, but their solubility is remarkably low, due to the strong hydrophobicity of hydrocarbon groups. The sharp comparison suggests that *the small dissociation constant of supporting electrolytes in organic solvents is the root cause for the low conductivity of their solutions*. This highlights the need

for the development of high-relative permittivity organic solvents for electrochemical applications with respect to improving the conductivity for supporting electrolytes.

3.5. Toxicity and other considerations

The toxicity of organic solvents is also an important consideration. The median lethal dose ($\mathbf{LD_{50}}$) is used to compare the toxicity of different organic solvents. In general, an $\mathbf{LD_{50}}$ value of 0.5−5.0 g_{oral} kg_{rat}^{-1} is considered to be slightly toxic. Note that the organic solvents with lower than 0.5 g_{oral} kg_{rat}^{-1} are not included for **Table 1**, because of the strong toxic concerns. One should use low or less toxic solvents at all possible circumstances. In addition to the $\mathbf{LD_{50}}$, other toxicity parameters should also be considered in selecting organic solvents.

The saturated vapour pressure (p^*) is also important in evaluating the toxicity of organic solvents. The lower p^* is, the less concern there is over possible solvent intake when handling. Most of organic solvents are flammable and a low p^* can also help reduce the fire risk.

Similar to viscosity, the density of the organic solvent affects the pumping cost. The density is also related to the specific energy: lower density leads to higher specific energy at a given cell voltage and capacity.

Organic solvents can be used in their pure form, but can also be used as mixtures for which possible combinations are almost unlimited. The engineering of these mixed solvents may provide unique properties that are not available from pure solvents for nonaqueous RFB applications as has been practiced successfully in lithium-based rechargeable batteries.[57]

3. Supporting electrolytes

3.1. Overview

In general, pure solvents have extremely low ionic conductivity (Λ_s stands for the ionic conductivity of pure solvent). Pure water has a Λ_s of 6×10^{-8} S cm^{-1}, and pure organic solvents also have extremely low ionic conductivities. For instance, pure PC and AN solvent have a Λ_s of 1×10^{-8} and 6×10^{-10} S cm^{-1}, respectively.[52] As such, a supporting electrolyte is necessary for organic solvents to provide sufficient ionic conductivity.

A supporting electrolyte consists of the supporting cation(s) and the supporting anion(s), both of which contribute ionic conductivity to their solutions. Each supporting ion has a certain ability to offer ionic conductivity, evidenced by its distinctive limiting molar conductivity in a given solvent (**Table 2**). Following the Stokes' law, smaller ionic radius of supporting ions leads to higher limiting molar conductivity. Note that the Stokes' law applies to most of the common supporting cations and anions, but it does not hold for small alkali metal cations (e.g., Li^+) and halogen anions in terms of their ionic radii. The limiting molar conductivity of metal alkali cations and halogen anions is smaller than that predicted by the Stokes' law, which is generally rationalized by the strong interaction between those ions and organic solvents. In addition, halogen anions are less electrochemically stable than the supporting anions shown in **Table 2**, and thus they are rarely used in nonaqueous electrochemistry applications.

3.2. Supporting anions

Tetrafluoroborate (BF_4^-), perchlorate (ClO_4^-), and hexafluorophophate (PF_6^-) are the most often used supporting anions, since they have the smallest ionic radii (r: 0.229, 0.237, and 0.254 nm, respectively) and thus the highest limiting ionic conductivities (e.g., Λ_m: 108.5, 103.6, and 102.8 S cm^2 mol^{-1}, respectively, in AN, **Table 2**). The trend is the same for other solvents but limiting molar conductivity is smaller due to the large solvent viscosity. Special consideration should be given to the use of ClO_4^- supporting anion, because most perchlorate salts are of explosion concern when heated or shocked; and thus the safer BF_4^- and PF_6^- anions are strongly recommended. For benchmark, Cl^- supporting anion in water has a comparable limiting molar conductivity (Λ_m: 76.35 S cm^2 mol^{-1} in water). Note that some aqueous RFBs may use OH^- as working ion that has the highest limiting molar conductivity (Λ_m: 198.0 S cm^2 mol^{-1} in water) among all known anions.

The limiting oxidation potentials (E_{ox}) of those common supporting anions overlap with those of some common organic solvents (e.g., E_{ox}: 2.9−5.4 V vs. SHE, **Table 1**). In particular, the limiting oxidation potentials of FP_6^-, AsF_6^-, and BF_4^- are among the highest, e.g., E_{ox}: 3.6−3.8 V vs. SHE in PC (**Table 2**). It should be noted that AsF_6^- salts are highly toxic and PF_6^- salts are strongly recommended as supporting anion when possible. In general, supporting anions lose electrons to form radicals when electrode potential is higher than their limiting oxidation potentials and the radicals may further react with solvents. As such, the oxidation of supporting ions is irreversible (similar to solvent breakdown). The electrochemical window of a supporting electrolyte-containing organic solvent solution is determined by either supporting ions or solvent, whichever is limiting. The interaction between supporting ions and organic solvents may exist and the practical electrochemical window for their solution may differ.

3.3. Supporting cations

Tetraalkylammoniums are commonly used supporting cations, with Et_4N^+ and Bu_4N^+ being the two most popular cations. Similar to anions, smaller ionic radius of supporting cations leads to higher limiting molar conductivity. In particular, Me_4N^+, Et_4N^+, and Pr_4N^+ cations have smallest ionic radii (r: 0.283, 0.343, and 0.381 nm, respectively), and thus highest limiting molar conductivity (e.g., Λ_m: 94.52, 85.19, and 70.20 S cm^2 mol^{-1}, respectively, in AN, **Table 2**). The molar limiting conductivity of supporting cations is lower than that of supporting anions due to their larger ionic radius; and both supporting cations and supporting anions have similar molar limiting conductivity when they have close ionic radii (e.g., Λ_m: 61.63 vs. 58.02 S cm^2 mol^{-1} for Bu_4N^+ of 0.415 nm vs. BPh_4^- of 0.419 nm, **Table 2**). Metal cations are also used as supporting cations sometimes since they have simple cation structure and good reductive stability. Although Li^+ cation has the smallest ionic radius (r: 0.076 nm), its molar limiting conductivity is only close to that of Pr_4N^+ cation that has a much larger ionic radius (r: 0.381 nm). For benchmark in water, Na^+ has a limiting molar conductivity of 50.10 S cm^2 mol^{-1}. Note that some aqueous RFBs (e.g., aqueous all-vanadium RFBs) can use H^+ as working ions that has the highest limiting molar conductivity: (Λ_m: 349.81 S cm^2 mol^{-1}) among all known cations (and anions as well).

Unlike the supporting anions whose oxidative limiting potentials overlap with those of organic solvents, tetraalkylammonium supporting cations have slightly lower limiting reduction potential (E_{re}) than organic solvents: e.g., E_{re}: from −2.8 V to −2.9 V vs. SHE in PC. Note that the limiting reduction potentials of tetraalkylammonium cations are very close to that of Li^+ (E_{re}: −3.0 V vs. SHE in PC), suggesting

excellent reductive stability. Opposite to supporting anions that can lose electrons, tetraalkylammonium cations can gain electrons to form radicals when electrode potential is lower than their limiting reductive potentials. Combining supporting anions and supporting cations, supporting electrolytes overall can offer much wide electrochemical windows, such as 6.6 V (Bu_4NPF_6 in PC).

Compared with lower tetraalkylammonium cations (such as Me_4N^+ and Et_4N^+), higher counterparts (e.g., Pr_4N^+ and Bu_4N^+) have higher solubility especially in organic solvents that have a low relative permittivity (e.g., THF and DME). For example, Et_4NBF_4 has a solubility of less than 0.01 M in both THF and DME, but the solubility of Bu_4BF_4 is up to 2.02 and 1.70 M in THF and DME, respectively. For extremely low-relative permittivity solvents, like benzene, Am_4N^+ (tetraamylammonium) and Hex_4N^+ (tetrahexylammonium) are needed to have a decent solubility as supporting electrolytes.

Owing to the similar cationic structure and close ionic radius, tetraalkylphosphonium cations are similar to tetraalkylammonium cations in many ways including conductivity and stability. For example, Bu_4P^+ and Bu_4N^+ have similar limiting molar conductivity (Λ_m: 64.86[58] and 61.63 S cm^2 mol^{-1}, respectively, in AN) and the same limiting reductive potential (E_{re}: −2.8 V vs. SHE in PC)[59].

3.4. Concentration and competition

In organic solvents, different solutes are found to compete with each other. For instance, the solubility of Et_4NBF_4 is strongly influenced by the concentration of $V(acac)_3$ redox compound in AN solvent.[60] The higher concentration of $V(acac)_3$ redox compound, the lower solubility of Et_4NBF_4: The solubility of Et_4NBF_4 in AN decreases from 1.60 M without $V(acac)_3$, to 1.10 M with 0.2 M $V(acac)_3$, and further to 0.35 M with 0.5 M $V(acac)_3$. This phenomenon can be well explained by the theory of partial molar volume for solutes. The effect of competing solubility must be considered when choosing the concentration of supporting electrolytes.

Due to the strong interaction among ions at high concentration, the molar conductivity of supporting ions decreases with increasing concentration of supporting electrolyte (typically, via a cubic root of relationship).[61] On the other hand, increasing concentration of supporting electrolyte will increase dissociated free supporting ions (depending on its K_d). The two competing trends on conductivity can lead to a critical concentration of supporting electrolyte (if solubility is allowed) that reaches the highest ionic conductivity. For example, $LiClO_4$ was observed to have a critical concentration of around 0.7 M in PC at 25 °C, giving the highest ionic conductivity of 54 mS cm^{-1}.[62] Such a small critical concentration is caused by the strong interaction between Li^+ and solvent. For less-interacting ammonium cations, the critical concentration of their supporting electrolytes is much higher than Li^+ salts. For example, $MeEt_3NBF_4$ was shown to have a critical concentration higher than 2 M in the same PC solvent.[59] In the same work, Et_4NBF_4 showed a solubility of 1 M in PC, a value that has not reached the critical concentration yet.

4. Redox pairs

4.1. Overview

Two redox pairs are needed to construct an RFB cell, and the one with the lower redox potential serves as the negative redox pair and the other with the higher redox potential does as the positive redox pair. When charging or discharging, electrical energy is stored into or released from the combination of both redox pairs via the reductive-oxidative flipping of each pair simultaneously. The choice of redox pairs is crucial as it not only determines the cell voltage and electrode kinetics but also dictates the electrolyte cost and cell durability. There are two groups of redox pairs in nonaqueous RFBs: metal-based redox pairs and metal-free redox pairs.

4.2. Metal-based redox pairs

The use of metal-based redox pairs in nonaqueous RFBs is a natural extension of their success in aqueous RFBs. Unlike the simple metal ions in aqueous RFBs, metal-organic ligand coordination complexes are used to construct metal-based redox pairs in nonaqueous RFBs, largely because of the need for improving its solubility in organic solvents. Simple metal salts have very limited solubility in most organic solvents, but metal-organic ligand complexes are reasonably soluble in many organic solvents.

A metal-ligand complex is composed of a metal centre and several chelating ligands. The metals used to construct nonaqueous RFB pairs include Ru,[24, 63-65] Fe,[24, 29, 63, 64, 66] U,[25, 67-72] V,[26, 32, 60, 73-75] Cr,[28] Ni,[29, 66] Mn,[27] and Co.[30] Among those metals, V becomes increasingly attractive because it has good redox reversibility and moderate materials cost. Ru also shows good redox reversibility but its cost is prohibitive. For example, the retail price of $Ru(acac)_3$ is over 30 times higher than that of $V(acac)_3$, i.e., \$72.4/g vs. \$1.96/g, from Sigma-Aldrich (with the same ligand and the same purity of 97%). With the aim of reusing the massive amount of depleted and recovered radioactive elements form nuclear industry, Yamanura et al. has pioneered the use of U as redox pairs for nonaqueous RFBs. Fe, Cr, Mn, and Co are inexpensive and have the potential to drastically lower the materials cost for nonaqueous RFBs. However, these metals have poorer redox reversibility than Ru and V.

Based on the atoms that are directly linked to the metal centre, the organic ligands used to construct redox pairs can be categorized in several groups: double-oxygen bidentate ligands, double-nitrogen bidentate ligands, double-sulfur bidentate ligands, and hybrid-atom (oxygen and nitrogen) bidentate ligands.

Double-oxygen bidentate ligands include "acac" (acetylacetone),[25-28, 60, 63-65, 69, 72-75] "hfa" (hexafluroacetylacetone),[25] "tfa" (1,1,1-trifluoroacetylacetone), "fod" (hexaflurobutanoylpivaloylmethane),[25] "pta" (pivaloyltrifluoroacetone),[25] "ba" (benzoylacetone), "dpm" (dipivaloylmethane),[25] "btk" [m-bis(2,4-dioxo-1-pentyl)benzene],[67, 68, 71, 72] "etk" (8-oxo-2,4,12,14-acetylacetone),[67, 68, 72] and "acacen" [bis(acetylacetone)ethylenediamine].[30] Among those organic ligands, the "acac" is the most frequently used one to construct metal-organic coordination complexes as redox pairs for nonaqueous RFBs, since it is one of the simplest bidentate ligands that form strong coordination bonds with many transition metals.

The double-nitrogen bidentate ligand used includes "bpy" (2,2'-bipyridine),[24, 29, 63, 64, 66] and the double-sulfur bidentate ligand used includes "mnt" (maleonitriledithiolene),[32] Hybrid-atom bidentate ligand includes "tmma" (N,N,N',N'-tetramethylmalonamide)[70] where both oxygen atom and nitrogen atom serve as each dentate of the bidentate. In addition, there are monodentate ligands such as (single-oxygen)

"dmso" (dimethyl sulfoxide) and (single-oxygen) "dmf" (dimethylformamide).[25]

For oxygen-dentate ligands (such as acac), the metal in metal-ligand complexes offers the electron transfer via the change of its oxidation number upon redox reaction, in which ligands are redox-innocent. For nitrogen- (such as bpy) or sulphur-dentate ligands (such as mmt), both metal and ligand can provide electron transfer, in which ligands are redox-non-innocent. Combining different metals (with variable oxidation numbers) and different ligands (with variable substituents), metal-ligand complex redox pairs offer a wide range of redox potentials, shown in **Table 5**. Note that, the redox potential can be influenced substantially by both organic solvent and supporting electrolyte.[76]

The properties of metal-ligand coordination complexes are the result of the interactions between metals and ligands. As such it is difficult to compare one group of ligands to the others. Staying within the same group of ligands, the impact of ligand however can be revealed. For example, the increase of the basicity of oxygen-dentate ligand (via introducing electron-withdrawing substituents) can lead to the negative shift for the redox potential of U-oxygen-dentate ligand complexes: an increase of eight units of p*K*a value for basicity of ligands leads to a negative shift of roughly 500 mV for redox potential for U(VI)/U(V) complex redox pairs. It is expected that the rate constant of redox reaction will also be impacted, but the correlation has not been elucidated yet.

Generally speaking, the redox kinetics of metal-ligand complex redox pairs in nonaqueous solvents is more facile than that of simple metal ions-based redox pairs in aqueous system. As seen in **Table 5**, the standard rate constant is generally within the level of 10^{-3}~10^{-1} cm s^{-1} for most of metal-ligand complex redox pairs, which is statistically one to two orders of magnitude higher than those of aqueous metal ions-based redox pairs (a wide range of 10^{-6}~10^{-2} cm s^{-1}).[8] This can be rationalized by the fact that the electron transfer in metal-ligand complexes does not involve the change of coordinating groups.[77, 78] Facile redox kinetics can lower the electrode overpotential, which is useful for achieving high voltage efficiency.

Besides the metal-ligand complexes, polyoxometalates are an emerging class of redox compounds to serve as metal-based redox pairs in nonaqueous RFBs.[31] Polyoxometalates are polyatomic ions consisting of three or more transition metal oxyanions linked together by shared oxygen atoms to form a large, closed 3-dimensional framework. Two polyoxoxmetalate redox pairs were introduced recently by Anderson et al. for both aqueous and nonaqueous RFBs: $[SiV_3W_9O_{40}]^{10-}$/$[SiV_3W_9O_{40}]^{13-}$ with metal W being the electroactive element and $[SiV_3W_9O_{40}]^{7-}$/$[SiV_3W_9O_{40}]^{10-}$ with metal V being the electroactive element.[31] Both pairs offer up to three electrons of transfer upon redox reaction. With organic cations such as Bu_4N^+, these polyoxometaltes are soluble in many organic solvents. Considering many structures available, polyoxometalates may be a promising class of metal-based redox system to be explored for advancing nonaqueous RFBs.

4.3. Metal-free redox pairs

Redox pairs can also be constructed by metal-free organic redox compounds for nonaqueous RFBs (**Table 6**). Unlike the metal-based redox pairs, the electron transfer involves the formation of stable radicals. By gaining or losing electrons, neutral organic molecules can form radical anions or radical cations, respectively. In turns, the electron transfer between radical ions associated with neutral molecule lead to certain redox potentials. For example, the first proposed metal-free redox pairs for nonaqueous RFBs[33]: one pair constructed by neutral rubrene molecule and rubrene radical anion (i.e., Rubrene/Rubrene$^{\cdot-}$ with a redox potential of −1.9 V vs. SHE) and the other constructed by neutral rubrene molecule and rubrene radical cation (i.e., Rubrene$^{\cdot+}$/Rubrene with a redox potential of 1.4 V vs. SHE).

Most radicals are extremely reactive and thus short-lived, but there are many radicals that are relatively stable and sometimes persistent, and thus they could be used to construct metal-free redox pairs. From structural point of view, the stabilization of radicals can be through electronic resonance, steric crowding, and/or dimer formation.[79]

Besides rubrene, other metal-free redox compounds include 2,2,6,6-tetramethyl-1-piperidinyloxyl (TEMPO•, note this radical is neutral),[34] N-methylphthalimide (NMPI),[34] 1,5-bis(2-(2-(2-methoxyethoxy)ethoxy)ethoxy)anthracene-9,10-dione (15D3GAQ),[18] 2,5-di-tert-butyl-1,4-bis(2-methoxyethoxy)benzene (DBBB),[16] and a quinoxaline family[16] (**Table 6**). TEMPO• neutral radical is a classic persistent radical molecule, whose stability is provided by both steric crowding from four methyl groups and electronic resonance. NMPI•$^+$ cationic radical is stabilized through the electronic resonance with its electron-deficient benzene ring.[34] 15D3GAQ•$^-$ anionic radical is likely stabilized by the electronic resonance across two benzene rings.[80] DBBB•$^+$ cationic radical is largely stabilized via the electronic resonance from para-methoxy-benzene ring as extended conjugation system (steric crowding is also provided from two t-butyl substituents).[81] With different substituents, a group of quinoxaline redox compounds have been introduced and those quinoxaline anionic radicals are likely stabilized by their electronic resonance.

Considering the typical energy-storing time in RFBs being a few hours to up to a few days, the stability of radical-involving metal-free redox pairs may be sufficient. For example, up to 30 charge-discharge cycles have been demonstrated from a nonaqueous RFB based on a quinoxaline redox pair and a DBBB based redox pair, without substantially compromising either charge or discharge capacity.[16] Such cyclability suggests a great feasibility of using radical redox compound for nonaqueous RFBs.

The substituent of redox compounds has impacts not only on the redox potential but also on the redox activity for redox pairs. For example, electron-donating substituents are shown to lower the redox potential but enhance the redox activity for the Quinoxaline/Quinoxaline•$^-$ redox pair.[16] Note that the influence of substituent is expected to be different from anionic radicals and cationic radicals. Meanwhile, the substituent has significant impact on the solubility of redox compound. For instance, with two substituents of 2-(2-(2-methoxyethoxy)ethoxy)ethoxy, 15D3GAQ has a solubility five times higher than that of the substituent-free anthraquinone (Aq) (more than 0.25 M for 15D3GAQ vs. less than 0.05 M for Aq, in solvent PC).[18]

Based on variable redox radicals, metal-free redox pairs offer a wide range of redox potentials and a large rate constant, similar to metal-based redox pairs (**Table 6**). Like metal-based redox pairs, the electron transfer does not involve any bond forming or breaking, and hence the redox kinetics is very facile. Unlike the metal-based redox compounds whose solubility is generally limited (mostly less than 1 M), some metal-free redox compounds can offer very high solubility, with the example being substituent-free quinoxaline which has a solubility of 7 M in PC.[16]

Considering the huge number of stable radicals and with possible modifications by substituents, a great deal of possible choices of organic compound exists for constructing metal-free redox pairs for nonaqueous RFBs.

5. Urgent challenges

5.1. High internal resistance and low cell performance

A low internal resistance for an RFB cell is necessary to operate at high current density and to deliver high power density. However, the state-of-the-art nonaqueous RFBs have significantly high internal resistance, for which the low ionic conductivity of both the electrolyte and the membrane is primarily responsible.

The ionic conductivity is substantially lower for organic electrolytes than for aqueous solutions. For example, 1 M Et_4NBF_4 in AN has an ionic conductivity of 55.5 mS cm^{-1} (**Table 3**), which is only 65%, 27%, and 14% that of 1 M NaCl (85.76 mS cm^{-1}), 1 M KOH (209 mS cm^{-1}), and 1 M H_2SO_4 solution (394.5 mS cm^{-1}), respectively.[82] Such a low ionic conductivity of 55.5 mS cm^{-1} is equivalent to a resistance of 1.8 Ωcm^2 per 1 mm thickness of electrolyte and further a voltage loss of 180 mV per 100 mA cm^{-2} of current density.

The ionic conductivity of commercial ion-exchange membranes is also significantly lower in nonaqueous solutions than in aqueous solutions. For example, the ionic conductivity of typical commercial anion-exchange membranes (AEMs) in nonaqueous solution is around 0.2−0.5 mS cm^{-1}, e.g., 0.16 mS cm^{-1} for Neosepta AHA membrane from Tokuyama Co. in 0.1 M Et_4NBF_4-containing AN solution,[83] and 0.48 mS cm^{-1} for FAP4 membrane from Fuma-Tech in 1 M Et_4NBF_4-containing PC solution.[84] By contrast, the ionic conductivity of commercial AEMs in water is around 15 mS cm^{-1} for Cl^- and 40 mS cm^{-1} for OH^-; and the ionic conductivity of commercial cation-exchange membranes in water is around 20 mS cm^{-1} for Na^+ and 100 mS cm^{-1} for H^+. A conductivity level of 0.5 mS cm^{-1} will lead to a membrane resistance of 2.0 Ωcm^2 per 10 μm thickness of membrane and further a voltage loss of 200 mV per 10 μm thickness of membrane at 100 mA cm^{-2} of current density.

As a result, the overall resistance of current nonaqueous RFBs is prohibitively high, ranging from a few tens to a few hundreds of Ωcm^2, which drastically limits the discharge current density and discharge power density to up to only a few mA cm^{-2} and only a few mW cm^{-2}, respectively. Such a low current density and power density are two to three orders of magnitude lower than those of the state-of-the-art aqueous RFBs. Achieving low internal resistance and high cell performance is the most urgent need for developing nonaqueous RFBs with possible practical applications.

It is critical to lower the electrolyte resistance through advanced electrode design.[8] Reducing electrode thickness will directly lower electrolyte resistance inside electrode. Implementing flow-through electrode and engineering of electrode structure can also help, via increasing effective surface area and improving electrolyte transport. It is possible to design high-performance electrode by taking advantage of the great success of electrode engineering in aqueous RFBs.

It is also crucial to lower membrane resistance in nonaqueous solutions through improving ionic conductivity and reducing membrane thickness, yet without compromising ionic selectivity and other important requirements such as mechanic strength and chemical stability. It must be pointed out that the current commercial IEMs are not designed for nonaqueous electrochemical applications, and therefore there is substantial room to improve membrane performance via preparing membranes specifically-tailored for nonaqueous RFB applications. In our previous studies, multiple ion exchange membrane configurations were developed which allowed flexible choices of redox pairs with mixed ion charges and different electrolytes to construct RFBs (**Figure 2**).[22]

5.2. Sensitive redox system and limited cell durability

As for applications in renewable electricity storage, RFBs are required to have good cyclability and durability, and nonaqueous RFBs are not an exception. However, sufficient robustness of existing redox systems has not been demonstrated, toward which the stability of redox pairs and resilience of redox systems are the central focus.

Both electrochemical stability and chemical stability of redox pairs are the prerequisite for durable nonaqueous RFBs. Nonaqueous redox pairs possess high rate constants, suggesting a good electrochemical reversibility. However, their chemical stability can be of concern. For metal-based redox pairs, the organic ligands can be detached under certain circumstances. For metal-free redox pairs, the concern is their long-term chemical stability especially when nonaqueous RFBs are at the charged state.

It has been shown that oxygen and water from ambient atmosphere can also have substantial impacts on nonaqueous RFBs.[85] Oxygen can passivate electrode through reaction with both electrode materials and water deactivate redox pairs by forming oxo-metal complexes.

Designing and developing robust and resilient redox systems are also an urgent challenge for nonaqueous RFBs to be able to offer sufficient cyclability and durability for practical applications.

6. An example: designing a 4.5 V nonaqueous RFB

6.1. The idea and working principles

As discussed in the **Section 2**, nonaqueous RFBs may offer a wide range of working temperature, high cell voltage, and potentially high energy density. Herein we present an example of designing an ultrahigh-voltage (4.52 V) nonaqueous RFB with a high theoretical energy density (278 Wh L^{-1}) and wide working temperature (202 °C). Such a ultrahigh-voltage nonaqueous RFB is constructed by two redox pairs (one with ultra-negative redox potential in negative electrolyte, and the other with ultra-positive redox potential in positive electrolyte), and one Li^+-conducting ceramic membrane between negative electrolyte and positive electrolyte (**Figure 3**).

It has long been known that some aromatic hydrocarbons are able to form stable radical anions, creating reversible redox pairs with very negative redox potentials.[86-88] In particular, the biphenyl molecule (BP) can be reversibly reduced to form the biphenyl radical anion ($BP^{\bullet-}$), with a very negative redox potential, e.g., a half-wave reduction potential of –2.70 V vs. SCE (or –2.46 V vs. SHE) observed for $BP/BP^{\bullet-}$ redox pair in AN solvent. In addition, the comprehensive studies of both equilibrium constant of the reaction ($BP + Na = BP^{\bullet-}Na^+$) and dissociation constant of $BP^{\bullet-}Na^+$ salt suggest good redox reversibility and sufficient radical stability.[87]

On the other hand, a number of redox shuttle molecules have been recently explored with the main purpose of protecting lithium-ion batteries from being overcharged.[89, 90] Those redox shuttle compounds can form stable radical cations, leading to very positive redox potentials. In particular, the octafluoronaphthalene molecule

(OFN) can be reversibly oxidized to form the octafluoronaphthalene radical cation (OFN•$^+$), with a very positive redox potential, e.g., 4.85 V vs. Li^+/Li (or 1.85 V vs. SHE) measured for OFN•$^+$/OFN redox pair in a mixed carbonate solvent. In addition to the very high redox potential, 70 charging-discharging cycles were demonstrated for the OFN•$^+$/OFN redox pair in an experimental lithium-ion battery, which clearly demonstrated the stability of OFN•$^+$ radical cation.[91]

Herein our idea is to combine the BP/BP•$^-$ redox pair and the OFN•$^+$/OFN redox pair in RFB, which may promise to achieve unprecedentedly high cell voltage. DMF and PC are carefully chosen as organic solvent for the two pairs, respectively, with criteria of both good electrochemical reversibility and high solubility.

6.2. Electrochemistry

The electrochemistry of both redox pairs was checked by performing cyclic voltammetry (CV) on a micro-Pt disk working electrode in their corresponding nonaqueous solvents, and Pt wire and Ag wire were used as counter electrode and reference electrode, respectively.

Figure 4A shows CV curves of 0.1 M BP in DMF solvent (0.1 M Bu_4NClO_4 as supporting electrolyte, argon atmosphere). Regardless of scan rate, every CV curve of BP shows a cathodic CV peak (i.e., BP reduction: BP + e^- = BP•$^-$, around –2.3 V vs. Ag wire) and an anodic one (i.e., BP•$^-$ oxidation: BP•$^-$ = BP + e^-, around –2.2 V vs. Ag wire), which leads to the formal redox potential of –2.25 V vs. Ag wire for the BP/BP•$^-$ redox pair (or –1.71 V vs. SHE assuming the potential of Ag wire of 0.54 V vs. SHE). Such a redox potential is 0.8+ V more negative than that of the Rubrene/Rubrene•$^-$ (–0.9 V vs. SHE, **Table 6**).

Both cathodic peak current and anodic one increased with scan rate, and the diffusion coefficient of BP was obtained by using the Randles-Sevcik equation for reversible systems. **Figure 4B** shows the fitting of the cathodic peak current against the square root of scan rate, giving a diffusion coefficient of 1.1×10^{-5} cm^2 s^{-1} for BP. Furthermore, the standard rate constant of BP/BP•$^-$ redox pair was also estimated by using the Nicholson method.[92] **Table S1** shows the standard rate constant for each CV curve and the standard rate constant averages 4.8×10^{-3} cm s^{-1} for BP/BP•$^-$ redox pair. Although this value is lower than those of some reported metal-free redox pairs in **Table 6**, overall the kinetics is very facile. The obtained formal potential, diffusion coefficient, and standard rate constant of BP/BP•$^-$ redox pair are summarized in **Table 7**.

Figure 4D shows CV curves of 0.1 M OFN in PC (0.1 M Bu_4NClO_4 as supporting electrolyte, argon atmosphere). Similarly, every CV curve shows an anodic CV peak (i.e., OFN oxidation: OFN = OFN•$^+$ + e^-, around 2.3 V vs. Ag wire) and a cathodic one (i.e., OFN•$^+$ reduction: OFN•$^+$ + e^- = OFN, around 2.2 V vs. Ag wire). The two CV peaks defines the formal redox potential as 2.27 V vs. Ag wire (or 2.81 V vs SHE assuming the potential of Ag wire of 0.54 V vs. SHE) for the OFN•$^+$/OFN redox pair. Such a redox potential is 1.4+ V more positive than that of Rubrene•$^+$/Rubrene redox pair (1.4 V vs. SHE, **Table 6**). Note that combining both BP/BP• redox pair and OFN•$^+$/OFN redox pair in an RFB cell may lead to a standard cell voltage of 4.52 V (**Figure 3**), which is the highest among all reported nonaqueous RFBs.

Using the same Randles-Sevcik equation for reversible systems, the anodic CV peak current against the square root of scan rate is plotted (**Figure 4E**), giving a diffusion coefficient of OFN of 4.2×10^{-8} cm^2 s^{-1}. Note that such a diffusion coefficient of OFN in PC is much lower than that of BP in DMF (1.1×10^{-5} cm^2 s^{-1}), and this difference can be in part explained by the stronger solvent viscosity (2.53 vs. 0.92 mPa·s for PC vs. DMF, **Table 1**) and the larger molecular weight (272.09 vs. 154.21 g mol^{-1} for OFN vs. BP). The standard rate constant of OFN•$^+$/OFN redox pair was also obtained by using the same Nicholson method, and **Table S2** shows the standard rate constant of each CV curve. The average standard rate constant is 1.7×10^{-3} cm s^{-1} for OFN•$^+$/OFN redox pair. Despite the big difference in diffusion coefficient of the neutral molecule, the standard rate constant of the OFN•$^+$/OFN redox pair is relatively close to that of the BP/BP•$^-$ redox pair (4.8×10^{-3} cm s^{-1}). Such a high level of standard rate constant (> 10^{-3} cm s^{-1}) suggests that both pairs are sufficient for RFB applications.

6.3. Solubility and temperature

The NMR spectroscopy method was used to determine the solubility of redox compounds in organic solvents (^{1}H NMR for BP, **Figure S1**; and ^{13}C NMR for OFN, **Figure S2**). **Figure 4C** shows the NMR-detected BP concentration in DMF solution against the apparent concentration of added BP. Before saturation, the detected BP concentration linearly increased with the added BP in the solution, and the detected BP levelled off when the added BP is high enough. Since only truly-soluble species in solution can be detected by NMR spectroscopy, the observed saturated concentration is the solubility of BP in DMF: 9.7 mol L^{-1}. Similarly, the **Figure 4F** shows the detected OFN concentration in PC solution against the apparent concentration of the added OFN. The observed solubility of OFN in PC was 3.0 mol L^{-1}. Both solubility values are listed in **Table 7**.

Such high solubility values may lead to a theoretical capacity density of 61.4 Ah L^{-1} for the BP-OFN nonaqueous RFB. Note that this theoretical capacity density is solely based on the neutral redox compounds and pure solvents, not accounting for the supporting electrolytes or the possible solubility changes of their radical ions. Considering the ultrahigh cell voltage of 4.52 V, such a high capacity density may further lead to an unprecedented theoretical energy density of 278 Wh L^{-1}.

Under ambient pressure, DMF has a freezing point of –60 °C and a boiling point of 153 °C, and PC has a freezing point of –49 °C and a boiling point of 242 °C. Without considering the effects of freezing point suppression and boiling point elevation (discussed in **Section 3.1**), the BP–OFN nonaqueous RFB may operate at the working temperature between –49 °C and 153 °C, or as wide as 202 °C.

The full-cell design and assembly, utilizing both BP/BP•$^-$ redox pair and OFN•$^+$/OFN redox pair, is currently under investigation and the results will be published in due course.

7. Concluding remarks

Here we highlight the key features of nonaqueous RFBs and focus on their major components: organic solvent, supporting electrolyte, and redox pairs. As a member of the RFB family, nonaqueous RFBs, especially those with the ability to work at low temperatures, are an important complement of aqueous RFBs, extending the range of RFB applications. Achieving low internal resistance and designing robust redox systems represent the two urgent needs for developing viable nonaqueous RFBs with high cell performance and good durability. To advance nonaqueous RFBs, it is important to understand both components and the system; and the understanding can be best achieved by collaborations across disciplines including electrochemistry, organic chemistry, physical chemistry, cell design, and system engineering. In order to demonstrate key features of nonaqueous RFBs, we also present an example of designing a 4.5 V ultrahigh-voltage nonaqueous RFB by combining BP/BP•$^-$ redox pair and ONF•$^+$/OFN redox pair.

Energy & Environmental Science RSCPublishing

PERSPECTIVE

Table 1 Low-freezing-point organic solvents of possible choices for nonaqueous RFBs

Solvent	T_f[a] (°C)	T_b[b] (°C)	d[c] (g cm^{-3})	μ[d] (mPa·s)	ε_r[e] (−)	LD_{50}[f] (g_{oral} kg_{rat}^{-1})	p^*[g] (kPa)	E_{red}[h] (V vs. SHE)	E_{oxi}[i] (V vs. SHE)	ECW[j] (V)
N,N-Dimethylacetamide (DMAc)	−20	166	0.94	0.93	37.8	4.30	9.77			
N-Methyl-2-pyrrolidone (NMP)	−24	204	1.03	1.70	32.2	3.90	0.84			
Nitromethane (NM)	−29	101	1.13	0.61	36.7	0.94	4.88	−1.0	2.9	3.9
γ-Valerolactone (GVL)	−31	208	1.05	2.00	42.0	8.80	0.027	−2.8	5.4	8.2
Methoxyacetonitrile (MAN)	−35	120	0.96	0.70	36.0	0.98	2.50	−2.5	3.2	5.7
γ-Butyrolactone (GBL)	−43	204	1.13	1.73	39.1	1.54	0.43	−2.8	5.4	8.2
Acetonitrile (AN)	−44	82	0.79	0.34	35.9	4.01	11.81	−2.6	3.5	6.1
Trimethyl phosphate (TMP)	−46	197	1.07	2.20	21.0	0.84	0.13	−2.7	3.7	6.4
Propylene carbonate (PC)	−49	242	1.20	2.53	64.9	5.00	0.017	−2.8	3.8	6.6
1,2-Butylene carbonate (BC)	−53	240	1.14	3.20	53.0	5.00	0.0056	−2.8	4.4	7.2
3-Methoxypropionitrile (MPN)	−57	165	0.94	1.10	36.0	4.39	0.28	−2.5	3.3	5.8
N,N-Dimethylformamide (DMF)	−60	153	0.94	0.92	36.7	2.80	0.49			
Diglyme	−64	160	0.94	0.99	7.23	5.40	0.45			
1,2-Dimethoxyethane (DME)	−69	85	0.86	0.46	7.20	5.37	6.38			
4-Methyl-2-pentanone	−84	117	0.80	0.55	13.1	2.08	2.50			
Ethyl acetate (EA)	−84	77	0.89	0.43	6.02	5.62	12.57			
2-Propanol	−88	82	0.78	2.04	19.9	5.05	5.76			
Nitroethane (NE)	−90	115	1.05	0.68	28.0	1.10	2.08	−1.1	3.2	4.5
Toluene	−95	111	0.86	0.55	2.38	5.58	3.79			
Hexane	−95	69	0.65	0.29	1.88	25.00	20.12			
Acetone	−95	56	0.78	0.30	20.6	1.80	30.72			
Dichloromethane (DCM)	−95	40	1.32	0.39	8.93	2.00	57.99			
Methanol (MeOH)	−98	65	0.79	0.55	32.7	1.98	16.89			
Tetrahydrofuran (THF)	−108	66	0.89	0.46	7.58	2.45	21.55			
Ethanol (EtOH)	−115	78	0.78	1.08	24.6	7.06	7.85			
1-Propanol	−126	97	0.80	1.94	20.5	8.04	2.79			

[a] T_f: freezing point of pure solvent and data from Ref.[52]
[b] T_b: boiling point of pure solvent and data from Ref.[52]
[c] d: density and data from Ref.[52]
[d] μ: viscosity and data from Ref.[52]
[e] ε_r: relative permittivity and data from Ref.[52]
[f] LD_{50}: median lethal dose (50%), data from Material Safety Data Sheets of Sigma-Aldrich.
[g] p^*: saturated vapour pressure at room temperature and data from Ref.[52]
[h] E_{red}: limiting reduction potential (0.65 M Et_4NBF_4, 25 °C, glassy carbon, 5 mV s^{-1}, and 1 mA cm^{-2} as threshold) and data from Ref.[59] The potential is converted by SCE = 0.24 V vs. SHE.
[i] E_{oxi}: limiting oxidation potential (0.65 M Et_4NBF_4, 25 °C, glassy carbon, 5 mV s^{-1}, and 1 mA cm^{-2} as threshold) and data from Ref.[59] The potential is converted by SCE = 0.24 V vs. SHE.
[j] **ECW**: electrochemical window (ECW = $E_{ox} - E_{re}$).

Table 2 Limiting molar conductivity of supporting ions in organic solvent with distinctive viscosity

Supporting ion		$r^{[a]}$ (nm)	$\Lambda_m^{[b]}$ (S cm^2 mol^{-1})					$E_{re}^{[c]}$ (V vs. SHE)	$E_{ox}^{[d]}$ (V vs. SHE)
			PC (μ: 2.53 mPa·s)	GBL (μ: 1.73 mPa·s)	H_2O (μ: 0.89 mPa·s)	THF (μ: 0.46 mPa·s)	AN (μ: 0.34 mPa·s)		
Anion	BF_4^-	0.229	20.43	30.77	75.1[93]		108.5[94]		3.6
	ClO_4^-	0.237	18.93	28.45	67.36	88.9[95]	103.6		3.1
	PF_6^-	0.254	17.86	26.70	65.5[93]	77.5[96]	102.8[97]		3.8
	AsF_6^-	0.260	17.58	25.92	32.4[98]		100.1[97]		3.8
	$CF_3SO_3^-$	0.270	16.89	24.93			96.3		3.0
	$(CF_3SO_2)_2N^-$	0.325	14.40	20.55	32.2[99]		83.72[99]		3.3
	$C_4F_9SO_3^-$	0.339	13.03	18.66					3.3
	BPh_4^-	0.419	8.52	11.67	19.8[100]		58.02		1.0
Cation	Li^+	0.076	8.43	13.99	38.68		69.97[97]	−3.0	
	Me_4N^+	0.283	14.50	21.52	44.9		94.52	−2.9	
	Et_4N^+	0.343	13.50	19.32	32.7		85.19	−2.8	
	Pr_4N^+	0.381	10.47[101]		23.45[102]		70.20[103]	−2.8	
	Bu_4N^+	0.415	9.09	14.03	19.5	43.8[96]	61.63	−2.8	
	Am_4N+	0.467[101]	8.05[101]		17.13[102]		55.81[104]		
	Hex_4N^+	0.469[105]	6.14[105]				50.58[104]	−2.9	

[a] r: ionic radius and data from the Ref.[106]

[b] Λ_m: limiting molar conductivity at 25 °C, data in solvents PC and GBL from the Ref.[106], solvents EtOH and AN from Ref.[52]

[c] E_{re}: limiting reduction potential, data from the Ref.[59] (BF_4^- as supporting anion, 0.65 M, 25 °C, glassy carbon, 5 mV s^{-1}, and 1 mA cm^{-2} as threshold). The potential is converted by SCE = 0.24 V vs. SHE. Caution is needed for using the potential conversion.

[d] E_{ox}: limiting oxidation potential, data from the Ref.[107] (Et_4N^+ as supporting cation, 0.65 M, 25 °C, glassy carbon, 5 mV s^{-1}, and 1 mA cm^{-2} as threshold). The potential is converted by Li^+/Li = −3.00 V vs. SHE.

Table 3 Solubility and conductivity of common tetraalkyammonium supporting electrolytes in some organic solvents[a]

Supporting electrolyte		S[b] (mol L^{-1})				σ_{1M}[c] (mS cm^{-1})			
		DMF (ε_r: 36.7)	AN (ε_r: 35.9)	THF (ε_r: 7.58)	DME (ε_r: 7.20)	DMF (ε_r: 36.7; μ: 0.92 mPa·s)	AN (ε_r: 35.9; μ: 0.34 mPa·s)	THF (ε_r: 7.58; μ: 0.46 mPa·s)	DME (ε_r: 7.20; μ: 0.46 mPa·s)
Bu_4N^+ salt	Bu_4NBF_4	2.34	2.21	2.02	1.70	14.5	32.3	2.7	4.4
	Bu_4NClO_4	2.29	2.05	1.48	1.10	12.0[59]	27.0[59]	2.7	3.2
	$Bu_4NCF_3SO_3$	2.25	2.50	2.35	–	10.9	23.3	3.3	–
Et_4N^+ salt	Et_4NBF_4	1.24	1.69	< 0.01	< 0.01	26.3	55.5	–	–
	Et_4NClO_4	1.00	1.13	< 0.01	< 0.01	24.0[59]	50.0[59]	–	–
	$Et_4NCF_3SO_3$	2.58	3.10	0.08	–	20.8	41.7	–	–

[**a**] All data in this table are from the Ref.[52], unless otherwise noted.
[**b**] S: solubility of supporting electrolyte.
[**c**] σ_{1M}: conductivity of the solution with 1 M supporting electrolyte.

Table 4 Dissociation constant of supporting electrolytes in organic solvents with distinctive relative permittivity

Supporting electrolyte		$\log[K_d/(\text{mol } L^{-1})]$[a]				
		PC (ε_r: 64.9)	GBL (ε_r: 39.1)	AN (ε_r: 35.9)	DCM (ε_r: 8.93)	THF (ε_r: 7.58)
Bu_4N^+ salt	Bu_4NBF_4			−1.08[108]		
	Bu_4NClO_4	−0.45	−0.94	−1.58[96]	−4.53[96]	−5.71[96]
	Bu_4NPF_6			−1.55[96]	−3.19[54]	−5.57[96]
	Bu_4BPh_4	−0.38	−0.80	−1.04[109]	−2.71[54]	−3.68[54]
Et_4N^+ salt	Et_4NBF_4	−0.48	−1.00		−4.69[110]	
	Et_4NClO_4	−0.49	−0.98		−4.66[111]	
	Et_4NPF_6	−0.30	−0.89		−4.61[110]	
	$Et_4NCF_3SO_3$	−0.36	−0.98			
	$Et_4N(CF_3SO_2)_2N$	−0.26	−0.68		−4.50[110]	

[**a**] K_d: dissociation constant of supporting electrolyte. The K_d data are converted from data of association constant (K_a) by the equation $K_d = 1/K_a$. K_a data for solvents PC and GBL are from the Ref.[106]

Table 5 Metal-based redox pairs proposed in nonaqueous RFBs

Redox pair[a]	φ'[b] (V vs. SHE)	k_0[c] (cm s^{-1})	**Test condition**[d]
$[Ru(bpy)_3]^{3+}/[Ru(bpy)_3]^{2+}$	1.5 (from Ag^+/Ag)[24]	3.4×10^{-3} (from i_0[e])[112]	
$[Fe(bpy)_3]^{3+}/[Fe(bpy)_3]^{2+}$	1.3 (from SCE)[112]	1.3×10^{-2} (from i_0)[112]	
$[Ru(acac)_3]^+/Ru(acac)_3$	1.2 (from SCE)[112]	4.6×10^{-2} (from i_0)[112]	
$[Mn(acac)_3]^+/Mn(acac)_3$	1.2 (from Ag^+/Ag)[27]		0.5 M Et_4NBF_4
$[V(acac)_3]^+/V(acac)_3$	1.0 (from Ag^+/Ag)[26]	6.5×10^{-4} (DMSO, 0.05 M Et_4NPF_6)[74]	
$[Cr(acac)_3]^+/Cr(acac)_3$	1.0 (from Ag^+/Ag)[28]		0.5 M Et_4NBF_4
$[V(mnt)_3]^-/[V(mnt)_3]^{2-}$	0.9 (from Fc^+/Fc)[32]		0.1 M Bu_4NPF_6
$[Co(acacen)]^+/Co(acacen)$	0.3 (from Ag^+/Ag)[30]		0.1 M Et_4NPF_6
$Mn(acac)_3/[Mn(acac)_3]^-$	0.1 (from Ag^+/Ag)[27]		0.5 M Et_4NBF_4
$[V(mnt)_3]^{2-}/[V(mnt)_3]^{3-}$	−0.2 (from Fc^+/Fc)[32]		0.1 M Bu_4NPF_6
$[UO_2(dmso)_5]^-/[UO_2(dmso)_5]^{2-}$	−0.3 (from Fc^+/Fc)[25]		DMSO, 0.1 M Bu_4NClO_4, Pt
$[UO_2(hfa)_2]^-/[UO_2(hfa)_2]^{2-}$	−0.3 (from Fc^+/Fc)[25]		DMSO, 0.1 M Bu_4NClO_4, Pt
$[UO_2(tfa)_2]^-/[UO_2(tfa)_2]^{2-}$	−0.3 (from Fc^+/Fc)[25]		DMSO, 0.1 M Bu_4NClO_4, Pt
$[U(tmma)_4]^{4+}/[U(tmma)_4]^{3+}$	−0.4 (from Fc^+/Fc)[70]	4.8×10^{-7} [70]	DMF, 0.1 Bu_4NBPh_4, Pt
$Ru(acac)_3/[Ru(acac)_3]^-$	−0.5 (from SCE)[112]		
$[UO_2(fod)_2]^-/[UO_2(fod)_2]^{2-}$	−0.5 (from Fc^+/Fc)[25]		DMF, 0.1 M Bu_4NClO_4, Pt
$[UO_2(pta)_2]^-/[UO_2(pta)_2]^{2-}$	−0.5 (from Fc^+/Fc)[25]		DMSO, 0.1 M Bu_4NClO_4, Pt
$[SiV_3W_9O_{40}]^{7-}/[SiV_3W_9O_{40}]^{10-}$	−0.5 (from Li^+/Li)[31]		PC, 0.5 M Bu_4NOTf, GC
$[UO_2(ba)_2]^-/[UO_2(ba)_2]^{2-}$	−0.7 (from Fc^+/Fc)[25]		DMSO, 0.1 M Bu_4NClO_4, Pt
$UO_2(acac)_2/[UO_2(acac)_2]^-$	−0.8 (from Fc^+/Fc)[71]	7.7×10^{-3} [71]	DMSO, 0.1 M Bu_4NPF_6, GC
$[UO_2(dpm)_2]^-/[UO_2(dpm)_2]^{2-}$	−0.8 (from Fc^+/Fc)[25]		DMSO, 0.1 M Bu_4NClO_4, Pt
$UO_2(btk)/[UO_2(btk)]^-$	−0.8 (from Fc^+/Fc)[71]	1.03×10^{-3} [71]	DMSO, 0.1 M Bu_4NPF_6, GC
$UO_2(etk)/[UO_2(etk)]^-$	−0.8 (from Fc^+/Fc)[72]	1.1×10^{-2} [72]	DMSO, 0.1 M Bu_4NClO_4, GC
$[Ru(bpy)_3]^{2+}/[Ru(bpy)_3]^+$	−1.1 (from Ag^+/Ag)[24]	2.0×10^{-1} (DMF, 0.2 M Bu_4NClO_4, Pt)[113]	
$[Fe(bpy)_3]^{2+}/[Fe(bpy)_3]^+$	−1.1 (from SCE)[112]	1.6×10^{-1} (DMF, 0.2 M Bu_4NClO_4, Pt)[113]	
$V(acac)_3/[V(acac)_3]^-$	−1.2 (from Ag^+/Ag)[26]	8.7×10^{-4} (from i_0)[73]	0.5 M Et_4NBF_4
$[Ni(bpy)_3]^{2+}/Ni(bpy)_3$	−1.2 (from Ag^+/Ag)[66]		PC, 0.05 M Et_4NBF_4
$U(pta)_4/[U(pta)_4]^-$ (or $U(pta)_3$)	−1.3 (from Fc^+/Fc)[25]		DMSO, 0.1 M Bu_4NClO_4, Pt
$[V(mnt)_3]^{3-}/[V(mnt)_3]^{4-}$	−1.4 (from Fc^+/Fc)[32]		0.1 M Bu_4NPF_6
$Co(acacen)/[Co(acacen)]^-$	−1.7 (from Ag^+/Ag)[30]		0.1 M Et_4NPF_6
$U(btk)_2/[U(btk)_2]^-$	−1.8 (from Fc^+/Fc)[72]	8.8×10^{-3} [72]	DMF, 0.1 M Bu_4NClO_4
$U(acac)_4/[U(acac)_4]^-$ (or $U(acac)_3$)	−1.8 (from Fc^+/Fc)[72]	1.7×10^{-2} [72]	DMF, 0.1 M Bu_4NClO_4
$U(etk)_2/[U(etk)_2]^-$	−1.8 (from Fc^+/Fc)[72]	1.5×10^{-2} [72]	DMF, 0.1 M Bu_4NClO_4
$Cr(acac)_3/[Cr(acac)_3]^-$	−1.8 (from Ag^+/Ag)[28]		0.5 M Et_4NBF_4
$[SiV_3W_9O_{40}]^{10-}/[SiV_3W_9O_{40}]^{13-}$	−2.2 (from Li^+/Li)[31]		PC, 0.5 M Bu_4NOTf

[**a**] Full names of the ligand abbreviations: "bpy" stands for 2,2'-dipyridine, "acac" for acetylacetone, "mnt" for maleonitriledithiolene, dmso for dimethyl sulfoxide, "hfa" for hexafluroacetylacetone, "tfa" for 1,1,1-trifluoroacetylacetone, "tmma" for N,N,N',N'-tetramethylmalonamide, "fod" for hexaflurobutanoylpivaloylmethane, "pta" for pivaloyltrifluoroacetone, "ba" for benzoylacetone, "dpm" for dipivaloylmethane, "btk" for m-bis(2,4-dioxo-1-pentyl)benzene, "etk" for 8-oxo-2,4,12,14-acetylacetone, and "acacen" for bis(acetylacetone)ethylenediamine.

[**b**] φ': formal redox potential. Potential was converted to SHE scale by relationships: Ag^+/Ag = 0.54 V vs. SHE, SCE = 0.24 V vs. SHE, Li^+/Li = −3.00 V vs. SHE, and Fc^+/Fc = 0.69 V vs. SHE.[76] Caution is needed for using the potential conversion.

[**c**] k_0: standard rate constant of redox reaction.

[**d**] Test conditions are AN as solvent, 0.1 M Et_4NBF_4 as supporting electrolyte, and GC as electrode, unless otherwise noted.

[**e**] i_0: exchange current density.

Table 6 Metal-free redox pairs proposed in nonaqueous RFBs

Redox pair[a]	φ'[b] (V vs. SHE)	k_0[c] (cm s^{-1})	**Test conditions**[d]
Rubrene•$^+$/Rubrene	1.4 (from Ag wire)[33]		AN:Tol, 0.05 TBAP, GC
DBBB•$^+$/DBBB	1.0 (from Li^+/Li)[16]	1.0×10^{-2} (estimated)	
$TEMPO^+$/TEMPO•	0.9 (from Ag wire)[34]	1.0×10^{-1} (0.1 $TBABF_4$, Pt)[114]	AN, 1 M NaClO4, GC
Quinoxaline/Quinoxaline•$^-$	0.1 (from Li^+/Li)[16]		
DPh-quinoxaline/DPh-quinoxaline•$^-$	0.0 (from Li^+/Li)[16]		
Me-quinoxaline/Me-quinoxaline•$^-$	−0.1 (from Li^+/Li)[16]		
DMe-quinoxaline/DMe-quinoxaline•$^-$	−0.2 (from Li^+/Li)[16]		
TMe-quinoxaline/TMe-quinoxaline•$^-$	−0.2 (from Li^+/Li)[16]		
DPh-quinoxaline•$^-$/DPh-quinoxaline•$^{2-}$	−0.3 (from Li^+/Li)[16]		
Quinoxaline•$^-$/Quinoxaline•$^{2-}$	−0.4 (from Li^+/Li)[16]		
Me-quinoxaline•$^-$/Me-quinoxaline•$^{2-}$	−0.4 (from Li^+/Li)[16]		
15D3GAQ•$^-$/15D3GAQ^{2-}	−0.5 (from Li^+/Li)[18]		PC, 1 M $LiPF_6$, GF
DMe-quinoxaline•$^-$/DMe-quinoxaline•$^{2-}$	−0.5 (from Li^+/Li)[16]		
TMe-quinoxaline•$^-$/TMe-quinoxaline•$^{2-}$	−0.5 (from Li^+/Li)[16]		
15D3GAQ/15D3GAQ•$^-$	−0.8 (from Li^+/Li)[18]		1 M $LiPF_6$, GF
NMPI/NMPI•$^-$	−0.8 (from Ag wire)[34]	4.6×10^{-2} (0.1 $TBABF_4$, Pt)[115]	AN, 1 M NaClO4, GC
Rubrene/Rubrene•$^-$	−0.9 (from Ag wire)[33]		AN:Tol, 0.05 TBAP, GC

[**a**] Full names of the abbreviations: DBBB: 2,5-di-tert-butyl-1,4-bis(2-methoxyethoxy)benzene; TEMPO: 2,2,6,6-tetramethyl-1-piperidinyloxy; NMPI: N-methylphthalimide; 15D3GAQ: 1,5-bis(2-(2-(2-methoxyethoxy)ethoxy)ethoxy)anthracene-9,10-dione.

[**b**] φ': formal redox potential. Potential was converted to SHE scale by relationships: Ag^+/Ag = 0.54 V vs. SHE, and Li^+/Li = −3.00 V vs. SHE. Caution is needed for using the potential conversion.

[**c**] k_0: standard rate constant of redox reaction.

[**d**] Test conditions are PC as solvent, 0.2 M $LiPF_6$ as supporting electrolyte, and Pt as electrode, unless otherwise noted.

Table 7 Results of the BP/BP•$^-$ redox pair and the OFN•$^+$/OFN redox pair for nonaqueous RFBs

Redox pair	φ'[a] (V vs. SHE)	D[b] (cm^2 s^{-1})	k_0[c] (cm s^{-1})	S[d] (mol L^{-1})
BP/BP•$^-$	–1.71	1.1×10^{-5}	4.8×10^{-3}	9.7
OFN•$^+$/OFN	2.81	4.2×10^{-8}	1.7×10^{-3}	3.0

Test conditions for the BP/BP•$^-$ redox pair: DMF, 0.1 M BP, 0.1 M Bu_4NClO_4, Pt micro-working electrode (0.20 mm in diameter), Pt wire and Ag wire as counter electrode and reference electrode, respectively. Test conditions for the OFN•$^+$/OFN redox pair: PC, 0.1 M OFN, 0.1 M Bu_4NClO_4, all electrodes used were the same as the case of the BP/BP•$^-$ redox pair.

[**a**] φ': formal redox potential [$\varphi' = (\varphi_{pa} + \varphi_{pc})/2$, where φ_{pa} and φ_{pc} are the potential of anodic peak and the potential of cathodic peak, respectively.] The potential was converted to SHE scale by the relation: Ag wire = 0.54 V vs. SHE.

[**b**] D: diffusion coefficient of the neutral compound, i.e., BP molecule in DMF and OFN molecule in PC, obtained by using the Randles-Sevcik equation.

[**c**] k_0: standard rate constant of redox reaction, obtained by adopting the Nicholson method (**Tables S1** and **S2**).

[**d**] S: solubility of the neutral command, i.e., BP molecule in DMF and OFN molecule in PC, measured by employing ^{13}C NMR spectroscopy method (**Figures S1** and **S2**).

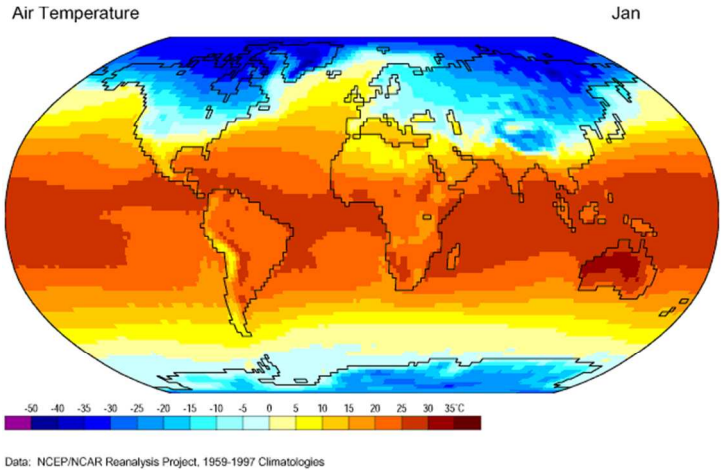

Figure 1. Mean air temperature in January on the Earth's surface (1959−1997). Source of Original Modified Image: Climate Lab Section of the Environmental Change Research Group, Department of Geography, University of Oregon - Global Climate Animations: *Digital Library for Earth System Education (Reviewed Collection)*, Permission to use this image has been generously granted from Prof. J. J. Shinker.

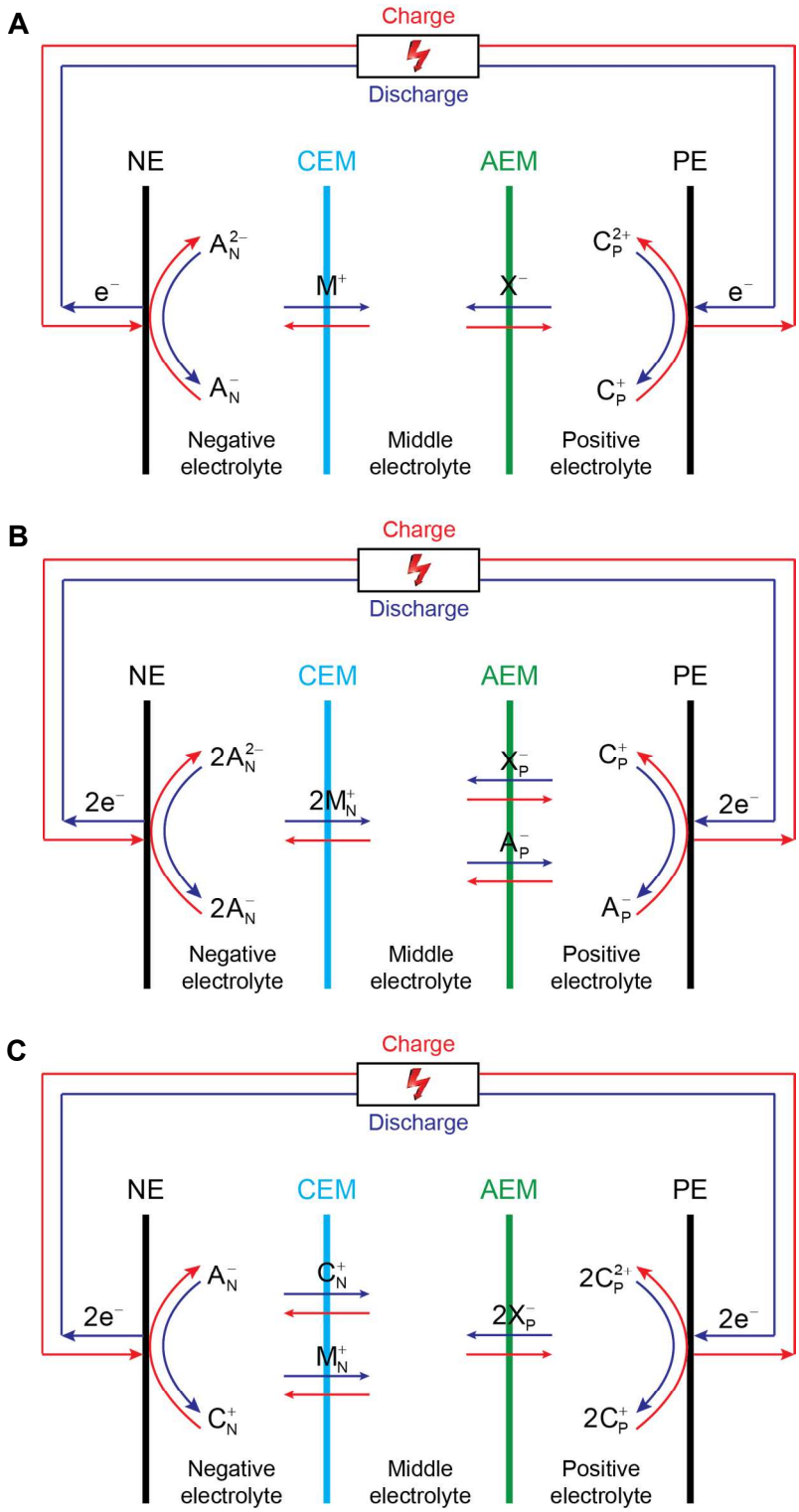

Figure. 2 Working principles of double-IEM RFB cell configuration. NE and PE represent the negative electrode and positive electrode, respectively. CEM and AEM stand for cation-exchange membrane and anion-exchange membrane, respectively. (**A**) Combination of an anion-anion (negative) redox pair (A_N^-/A_N^{2-}) and a cation-cation (positive) redox pair (C_P^{2+}/C_P^+). (**B**) Combination of an anion-anion (negative) redox pair (A_N^-/A_N^{2-}) and an anion-cation hybrid (positive) redox pair (C_P^+/A_p^-). (**C**) Combination of an anion-cation hybrid (negative) redox pair (C_N^+/A_N^-) and a cation-cation (positive) redox pair (C_P^{2+}/C_p^+). M^+, X^-, M_N^+, and X_P^- are balancing ions. Note that the general working principles are, for the sake of simplicity, based on the assumptions that cations with more positive charge have higher oxidation number than those with less positive charge, and anions with more negative charge have lower oxidation number than those with

less negative charge. When ions that do not follow those assumptions are used, the working principles are still applicable with minor alterations. (Reproduced with permission from Ref. 22)

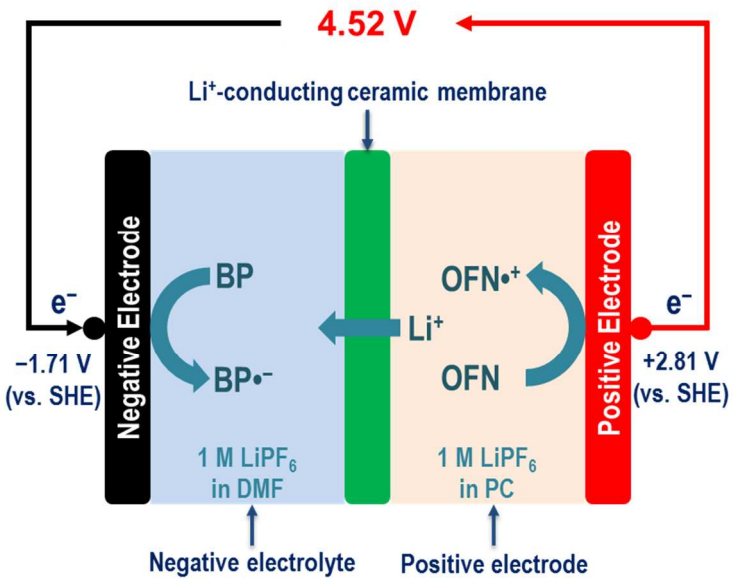

Figure 3. The BP-OFN nonaqueous RFB concept and its working principles. The negative electrolyte containing the BP/BP•$^-$ redox pair and the positive electrolyte containing the OFN•$^+$/OFN redox pair are separated by a Li^+-conducting ceramic membrane (e.g., LiSICON). 1 M $LiPF_6$ is used as an example of supporting electrolyte. When the cell is being charged, BP molecules are reduced to form BP•$^-$ radical anions in negative electrolyte (i.e., BP + e^- = BP•$^-$), and OFN molecules are oxidized to form OFN•$^+$ radical cations in positive electrolyte (i.e., OFN = OFN•$^+$ + e^-). Meanwhile, Li^+ ions pass through Li^+-conducting ceramic membrane from positive electrolyte to negative electrolyte. The discharging process is in reverse.

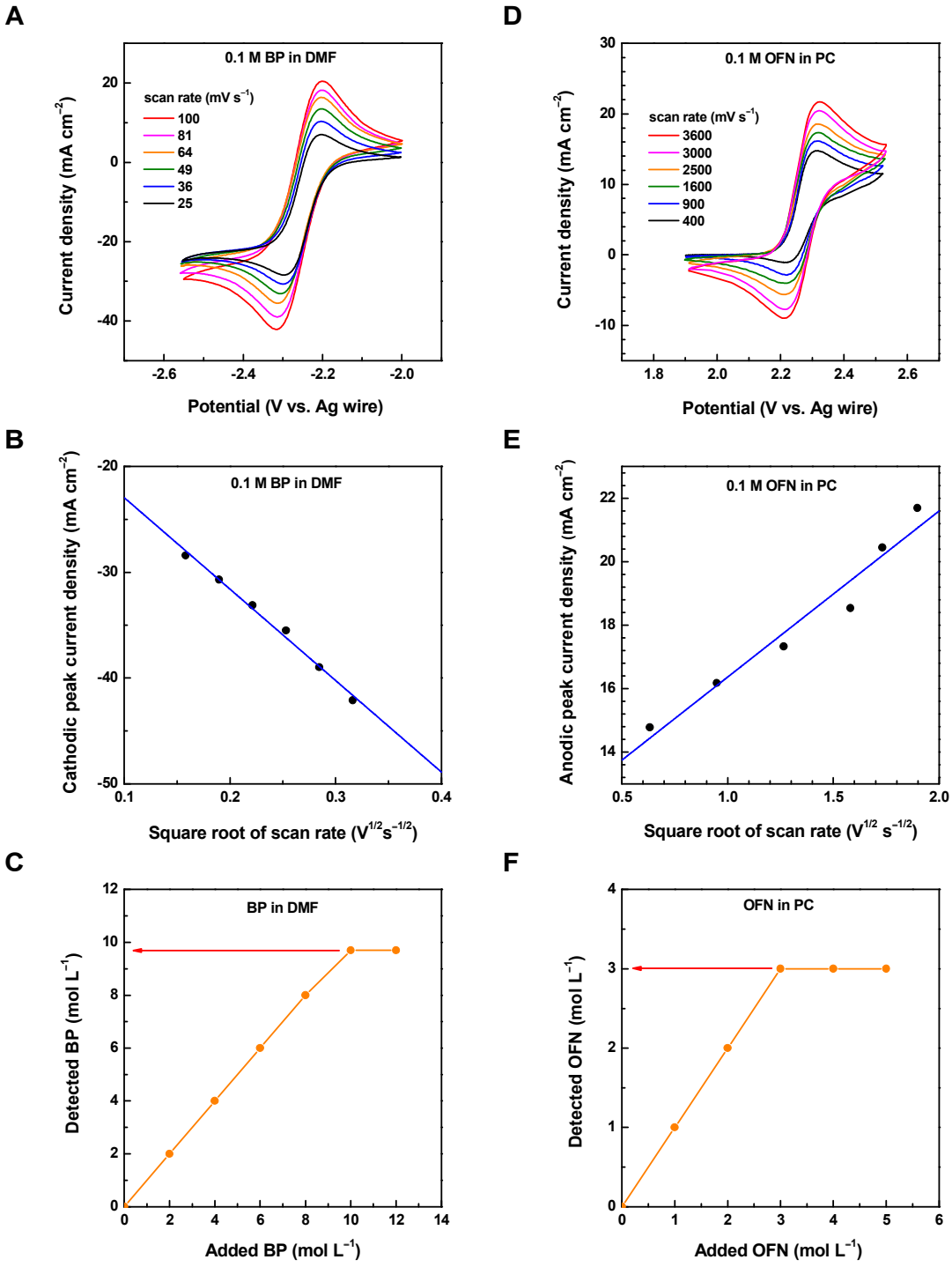

Figure 4. Electrochemistry and solubility of the BP/BP•$^{-}$ redox pair and the OFN•$^{+}$/OFN redox pair. (A) CV curves of BP/BP•$^{-}$ redox pair, test conditions: DMF solvent, 0.1 M BP, 0.1 M Bu_4NClO_4 as supporting electrolyte; Pt micro-working electrode (0.20 mm in diameter), and Pt wire and Ag wire as counter electrode and reference electrode, respectively. (B) Cathodic peak current density against the square root of scan rate for the BP/BP•$^{-}$ redox pair. (C) Solubility measurement of BP molecule in DMF solvent by NMR spectroscopy. (D) CV curves of OFN•$^{+}$/OFN redox pair, test conditions: PC solvent, 0.1 M OFN, 0.1 M. Bu_4NClO_4 as supporting electrolyte; Pt micro-working electrode (0.20 mm in diameter), and Pt wire and Ag wire as counter electrode and reference electrode, respectively. (E) Anodic peak current density against the square root of scan rate for the OFN•$^{+}$/OFN redox pair. (F) Solubility measurement of OFN molecule in PC solvent by NMR spectroscopy.

Acknowledgements

The work was supported in part by the Department of Energy of U.S. through ARPA-E program (DE-AR0000346).

Notes and references

[a] Department of Chemical and Biomolecular Engineering, Center for Catalytic Science and Technology, University of Delaware, Newark, DE 19716, USA.

[b] Department of Chemistry, National University of Singapore, Singapore 117543, Singapore.

Correspondence and requests for materials should be addressed to S.G. (email: shgu@udel.edu) or to Y.S.Y. (email: yanys@udel.edu)

† Footnotes should appear here. These might include comments relevant to but not central to the matter under discussion, limited experimental and spectral data, and crystallographic data.
Electronic Supplementary Information (ESI) available: [details of any supplementary information available should be included here]. See DOI: 10.1039/b000000x/

1. L. H. Thaller, *The 9th Intersociety Energy Conversion Engineering Conference Proceedings*, 1974, 924-928.
2. Z. G. Yang, J. L. Zhang, M. C. W. Kintner-Meyer, X. C. Lu, D. W. Choi, J. P. Lemmon and J. Liu, *Chem Rev*, 2011, **111**, 3577-3613.
3. B. Dunn, H. Kamath and J. M. Tarascon, *Science*, 2011, **334**, 928-935.
4. W. A. Braff, M. Z. Bazant and C. R. Buie, *Nat Commun*, 2013, **4**.
5. B. Huskinson, M. P. Marshak, C. Suh, S. Er, M. R. Gerhardt, C. J. Galvin, X. Chen, A. Aspuru-Guzik, R. G. Gordon and M. J. Aziz, *Nature*, 2014, **505**, 195-198.
6. C. P. de Leon, A. Frias-Ferrer, J. Gonzalez-Garcia, D. A. Szanto and F. C. Walsh, *J Power Sources*, 2006, **160**, 716-732.
7. M. Skyllas-Kazacos, M. H. Chakrabarti, S. A. Hajimolana, F. S. Mjalli and M. Saleem, *J Electrochem Soc*, 2011, **158**, R55-R79.
8. A. Z. Weber, M. M. Mench, J. P. Meyers, P. N. Ross, J. T. Gostick and Q. H. Liu, *J Appl Electrochem*, 2011, **41**, 1137-1164.
9. X. F. Li, H. M. Zhang, Z. S. Mai, H. Z. Zhang and I. Vankelecom, *Energ Environ Sci*, 2011, **4**, 1147-1160.
10. B. Schwenzer, J. L. Zhang, S. Kim, L. Y. Li, J. Liu and Z. G. Yang, *Chemsuschem*, 2011, **4**, 1388-1406.
11. P. Leung, X. H. Li, C. P. de Leon, L. Berlouis, C. T. J. Low and F. C. Walsh, *Rsc Adv*, 2012, **2**, 10125-10156.
12. W. Wang, Q. T. Luo, B. Li, X. L. Wei, L. Y. Li and Z. G. Yang, *Adv Funct Mater*, 2013, **23**, 970-986.
13. R. Ferrigno, A. D. Stroock, T. D. Clark, M. Mayer and G. M. Whitesides, *J Am Chem Soc*, 2002, **124**, 12930-12931.
14. Y. H. Lu, J. B. Goodenough and Y. Kim, *J Am Chem Soc*, 2011, **133**, 5756-5759.
15. Y. R. Wang, Y. G. Wang and H. S. Zhou, *Chemsuschem*, 2011, **4**, 1087-1090.
16. F. R. Brushett, J. T. Vaughey and A. N. Jansen, *Adv Energy Mater*, 2012, **2**, 1390-1396.
17. K. J. Kim, M. S. Park, J. H. Kim, U. Hwang, N. J. Lee, G. Jeong and Y. J. Kim, *Chem Commun*, 2012, **48**, 5455-5457.
18. W. Wang, W. Xu, L. Cosimbescu, D. W. Choi, L. Y. Li and Z. G. Yang, *Chem Commun*, 2012, **48**, 6669-6671.
19. Q. T. Luo, L. Y. Li, W. Wang, Z. M. Nie, X. L. Wei, B. Li, B. W. Chen, Z. G. Yang and V. Sprenkle, *Chemsuschem*, 2013, **6**, 268-274.
20. J. Liu, J. G. Zhang, Z. G. Yang, J. P. Lemmon, C. Imhoff, G. L. Graff, L. Y. Li, J. Z. Hu, C. M. Wang, J. Xiao, G. Xia, V. V. Viswanathan, S. Baskaran, V. Sprenkle, X. L. Li, Y. Y. Shao and B. Schwenzer, *Adv Funct Mater*, 2013, **23**, 929-946.
21. S. H. Shin, S. H. Yun and S. H. Moon, *Rsc Adv*, 2013, **3**, 9095-9116.
22. S. Gu, K. Gong, E. Z. Yan and Y. S. Yan, *Energ Environ Sci*, 2014, **7**, 2986-2998.
23. P. Singh, *J Power Sources*, 1984, **11**, 135-142.
24. Y. Matsuda, K. Tanaka, M. Okada, Y. Takasu, M. Morita and T. Matsumurainoue, *J Appl Electrochem*, 1988, **18**, 909-914.
25. T. Yamamura, Y. Shiokawa, H. Yamana and H. Moriyama, *Electrochim Acta*, 2002, **48**, 43-50.
26. Q. H. Liu, A. E. S. Sleightholme, A. A. Shinkle, Y. D. Li and L. T. Thompson, *Electrochem Commun*, 2009, **11**, 2312-2315.
27. A. E. S. Sleightholme, A. A. Shinkle, Q. H. Liu, Y. D. Li, C. W. Monroe and L. T. Thompson, *J Power Sources*, 2011, **196**, 5742-5745.
28. Q. H. Liu, A. A. Shinkle, Y. D. Li, C. W. Monroe, L. T. Thompson and A. E. S. Sleightholme, *Electrochem Commun*, 2010, **12**, 1634-1637.
29. J. H. Kim, K. J. Kim, M. S. Park, N. J. Lee, U. Hwang, H. Kim and Y. J. Kim, *Electrochem Commun*, 2011, **13**, 997-1000.
30. D. P. Zhang, H. J. Lan and Y. D. Li, *J Power Sources*, 2012, **217**, 199-203.
31. H. D. Pratt, N. S. Hudak, X. K. Fang and T. M. Anderson, *J Power Sources*, 2013, **236**, 259-264.
32. P. J. Cappillino, H. D. Pratt, N. S. Hudak, N. C. Tomson, T. M. Anderson and M. R. Anstey, *Adv Energy Mater*, 2014, **4**.
33. M. H. Chakrabarti, R. A. W. Dryfe and E. P. L. Roberts, *J Chem Soc Pakistan*, 2007, **29**, 294-300.
34. Z. Li, S. Li, S. Q. Liu, K. L. Huang, D. Fang, F. C. Wang and S. Peng, *Electrochem Solid St*, 2011, **14**, A171-A173.
35. S. Hamelet, T. Tzedakis, J. B. Leriche, S. Sailler, D. Larcher, P. L. Taberna, P. Simon and J. M. Tarascona, *J Electrochem Soc*, 2012, **159**, A1360-A1367.
36. M. Duduta, B. Ho, V. C. Wood, P. Limthongkul, V. E. Brunini, W. C. Carter and Y. M. Chiang, *Adv Energy Mater*, 2011, **1**, 511-516.
37. F. Y. Fan, W. H. Woodford, Z. Li, N. Baram, K. C. Smith, A. Helal, G. H. McKinley, W. C. Carter and Y. M. Chiang, *Nano Lett*, 2014, **14**, 2210-2218.
38. Y. H. Lu and J. B. Goodenough, *J Mater Chem*, 2011, **21**, 10113-10117.
39. Y. R. Wang, P. He and H. S. Zhou, *Adv Energy Mater*, 2012, **2**, 770-779.
40. N. M. Asl, S. S. Cheah, J. Salim and Y. Kim, *Rsc Adv*, 2012, **2**, 6094-6100.
41. Y. Zhao, L. N. Wang and H. R. Byon, *Nat Commun*, 2013, **4**.
42. J. Chun, M. Chung, J. Lee and Y. Kim, *Phys Chem Chem Phys*, 2013, **15**, 7036-7040.
43. Y. Y. Hou, X. J. Wang, Y. S. Zhu, C. L. Hu, Z. Chang, Y. P. Wu and R. Holze, *J Mater Chem A*, 2013, **1**, 14713-14718.

44. S. L. Chou, Y. X. Wang, J. T. Xu, J. Z. Wang, H. K. Liu and S. X. Dou, *Electrochem Commun*, 2013, **31**, 35-38.
45. Y. Zhao and H. R. Byon, *Adv Energy Mater*, 2013, **3**, 1630-1635.
46. Y. Zhao, M. Hong, N. B. Mercier, G. H. Yu, H. C. Choi and H. R. Byon, *Nano Lett*, 2014, **14**, 1085-1092.
47. J. K. Kim, W. Yang, J. Salim, C. Ma, C. W. Sun, J. Q. Li and Y. Kim, *J Electrochem Soc*, 2014, **161**, A285-A289.
48. P. Liu, Y. L. Cao, G. R. Li, X. P. Gao, X. P. Ai and H. X. Yang, *Chemsuschem*, 2013, **6**, 802-806.
49. N. F. Yan, G. R. Li and X. P. Gao, *J Electrochem Soc*, 2014, **161**, A736-A741.
50. R. M. Darling, K. G. Gallagher, J. A. Kowalski, S. Ha and F. R. Brushett, *Energ Environ Sci*, 2014, **7**, 3459-3477.
51. R. Matthé and U. Eberle, in *Lithium-Ion Batteries: Advances and Applications*, ed. G. Pistoia, Elsevier, 1st edn., 2014, ch. 8, pp. 151-176.
52. K. Izutsu, *Electrochemistry in Nonaqueous Solutions*, Wiley-VCH Verlag GmbH & Co. KGaA, Weinheim, Germany, 2009.
53. J. T. Denison and J. B. Ramsey, *J Am Chem Soc*, 1955, **77**, 2615-2621.
54. N. G. Tsierkezos and A. I. Philippopoulos, *Fluid Phase Equilibr*, 2009, **277**, 20-28.
55. F. J. Millero, *J Phys Chem-Us*, 1970, **74**, 356-&.
56. G. Petrella, M. Castagnolo, A. Sacco and A. Degiglio, *J Solution Chem*, 1976, **5**, 621-629.
57. K. Xu, *Chem Rev*, 2004, **104**, 4303-4417.
58. D. Ekka and M. N. Roy, *J Phys Chem B*, 2012, **116**, 11687-11694.
59. M. Ue, K. Ida and S. Mori, *J Electrochem Soc*, 1994, **141**, 2989-2996.
60. A. A. Shinkle, T. J. Pomaville, A. E. S. Sleightholme, L. T. Thompson and C. W. Monroe, *J Power Sources*, 2014, **248**, 1299-1305.
61. A. Chagnes, B. Carre, P. Willmann and D. Lemordant, *Electrochim Acta*, 2001, **46**, 1783-1791.
62. J. Barthel, H. J. Gores, R. Neueder and A. Schmid, *Pure Appl Chem*, 1999, **71**, 1705-1715.
63. M. H. Chakrabarti, R. A. W. Dryfe and E. P. L. Roberts, *Electrochim Acta*, 2007, **52**, 2189-2195.
64. M. H. Chakrabarti, E. P. L. Roberts and M. Saleem, *Int J Green Energy*, 2010, **7**, 445-460.
65. M. H. Chakrabarti, E. P. L. Roberts, C. Bae and M. Saleem, *Energ Convers Manage*, 2011, **52**, 2501-2508.
66. J. Mun, M. J. Lee, J. W. Park, D. J. Oh, D. Y. Lee and S. G. Doo, *Electrochem Solid St*, 2012, **15**, A80-A82.
67. T. Yamamura, K. Shirasaki, Y. Shiokawa, Y. Nakamura and S. Y. Kim, *J Alloy Compd*, 2004, **374**, 349-353.
68. Q. Sun, Q. Wang, Y. Shiokawa and Y. Kawazoe, *Chem Phys Lett*, 2005, **415**, 243-245.
69. K. Shirasaki, T. Yamamura, T. Herai and Y. Shiokawa, *J Alloy Compd*, 2006, **418**, 217-221.
70. T. Yamamura, K. Shirasaki, D. X. Li and Y. Shiokawa, *J Alloy Compd*, 2006, **418**, 139-144.
71. K. Shirasaki, T. Yamamura and Y. Shiokawa, *J Alloy Compd*, 2006, **408**, 1296-1301.
72. T. Yamamura, K. Shirasaki, H. Sato, Y. Nakamura, H. Tomiyasu, I. Satoh and Y. Shiokawa, *J Phys Chem C*, 2007, **111**, 18812-18820.
73. A. A. Shinkle, A. E. S. Sleightholme, L. T. Thompson and C. W. Monroe, *J Appl Electrochem*, 2011, **41**, 1191-1199.
74. T. Herr, J. Noack, P. Fischer and J. Tubke, *Electrochim Acta*, 2013, **113**, 127-133.
75. D. P. Zhang, Q. H. Liu, X. S. Shi and Y. D. Li, *J Power Sources*, 2012, **203**, 201-205.
76. N. G. Connelly and W. E. Geiger, *Chem Rev*, 1996, **96**, 877-910.
77. D. H. Evans, *Chem Rev*, 1990, **90**, 739-751.
78. D. H. Evans, *Chem Rev*, 2008, **108**, 2113-2144.
79. A. R. Forrester and R. H. Thomson, *Nature*, 1964, **203**, 74-&.
80. Z. P. Song, H. Zhan and Y. H. Zhou, *Chem Commun*, 2009, 448-450.
81. L. Zhang, Z. C. Zhang, P. C. Redfern, L. A. Curtiss and K. Amine, *Energ Environ Sci*, 2012, **5**, 8204-8207.
82. V. M. M. Lobo and J. L. Quaresma, *Handbook of Electrolyte Solutions*, Elsevier, Amsterdam, Netherlanda, 1989.
83. S. Maurya, S. H. Shin, K. W. Sung and S. H. Moon, *J Power Sources*, 2014, **255**, 325-334.
84. D. H. Kim, S. J. Seo, M. J. Lee, J. S. Park, S. H. Moon, Y. S. Kang, Y. W. Choi and M. S. Kang, *J Membrane Sci*, 2014, **454**, 44-50.
85. A. A. Shinkle, A. E. S. Sleightholme, L. D. Griffith, L. T. Thompson and C. W. Monroe, *J Power Sources*, 2012, **206**, 490-496.
86. S. Wawzonek and D. Wearring, *J Am Chem Soc*, 1959, **81**, 2067-2069.
87. N. L. Holy, *Chem Rev*, 1974, **74**, 243-277.
88. A. C. Aten, C. Buthker and G. J. Hoijtink, *T Faraday Soc*, 1959, **55**, 324-330.
89. C. Buhrmester, J. Chen, L. Moshurchak, J. W. Jiang, R. L. Wang and J. R. Dahn, *J Electrochem Soc*, 2005, **152**, A2390-A2399.
90. R. L. Wang and J. R. Dahn, *J Electrochem Soc*, 2006, **153**, A1922-A1928.
91. J. H. Chen, L. M. He and R. L. Wang, *J Electrochem Soc*, 2012, **159**, A1636-A1645.
92. Nicholso.Rs, *Anal Chem*, 1965, **37**, 1351-&.
93. H. Y. Wang, J. J. Wang, S. L. Zhang, Y. C. Pei and K. L. Zhuo, *Chemphyschem*, 2009, **10**, 2516-2523.
94. W. Libus, B. Chachulski and L. Fraczyk, *J Solution Chem*, 1980, **9**, 355-369.
95. O. N. Kalugin, V. G. Panchenko, A. P. Dolgareva, A. G. Nikolaichuk and I. N. V'yunnik, *Russ J Phys Chem a+*, 2008, **82**, 1480-1483.
96. R. J. LeSuer, C. Buttolph and W. E. Geiger, *Anal Chem*, 2004, **76**, 6395-6401.
97. F. Croce, A. DAprano, C. Nanjundiah, V. R. Koch, C. W. Walker and M. Salomon, *J Electrochem Soc*, 1996, **143**, 154-159.
98. A. Apelblat, *J Mol Liq*, 2010, **156**, 89-94.
99. M. Salomon, *J Solution Chem*, 1993, **22**, 715-725.
100. B. Das and D. K. Hazra, *J Solution Chem*, 1998, **27**, 1021-1031.
101. J. F. Reardon, *Electrochim Acta*, 1987, **32**, 1595-1600.
102. H. M. Daggett, E. J. Bair and C. A. Kraus, *J Am Chem Soc*, 1951, **73**, 799-803.
103. M. Salomon and E. J. Plichta, *Electrochim Acta*, 1984, **29**, 731-735.
104. B. S. Krumgalz, *J Chem Soc Farad T 1*, 1983, **79**, 571-587.
105. Y. Marcus, *Ion properties*, Marcel Dekker, Inc., New York, 1997.
106. M. Ue, *J Electrochem Soc*, 1994, **141**, 3336-3342.

107. M. Ue, M. Takeda, M. Takehara and S. Mori, *J Electrochem Soc*, 1997, **144**, 2684-2688.
108. I. Banik and M. N. Roy, *J Chem Thermodyn*, 2013, **63**, 52-59.
109. D. S. Gill, M. S. Chauhan and M. B. Sekhri, *J Chem Soc Farad T 1*, 1982, **78**, 3461-3466.
110. S. Katsuta, K. Imai, Y. Kudo, Y. Takeda, H. Seki and M. Nakakoshi, *J Chem Eng Data*, 2008, **53**, 1528-1532.
111. I. Svorstol, H. Hoiland and J. Songstad, *Acta Chem Scand B*, 1984, **38**, 885-893.
112. M. Morita, Y. Tanaka, K. Tanaka, Y. Matsuda and T. Matsumurainoue, *B Chem Soc Jpn*, 1988, **61**, 2711-2714.
113. T. Saji, T. Yamada and S. Aoyagui, *B Chem Soc Jpn*, 1975, **48**, 1641-1642.
114. T. Suga, Y. J. Pu, K. Oyaizu and H. Nishide, *B Chem Soc Jpn*, 2004, **77**, 2203-2204.
115. K. Oyaizu, A. Hatemata, W. Choi and H. Nishide, *J Mater Chem*, 2010, **20**, 5404-5410.

Electronic Supplementary Information for

Nonaqueous Redox-Flow Batteries: Organic Solvents, Supporting Electrolytes, and Redox Pairs

Ke Gong,[a] Qianrong Fang [a], Shuang Gu,[a,]* Sam Fong Yau Li,[b] and Yushan Yan[a,]*

[a] Department of Chemical & Biomolecular Engineering, Center for Catalytic Science and Technology, University of Delaware, Newark, DE 19716, USA.

[b] Department of Chemistry, National University of Singapore, Singapore 117543, Singapore.

Correspondence and requests for materials should be addressed to S.G. (email: shgu@udel.edu) or to Y.S.Y. (email: yanys@udel.edu)

1. Materials and methods

1.1. Cyclic voltammetry (CV)

Cyclic voltammetry (CV) was conducted in a 25 mL three-neck flask equipped with three electrodes under inert atmosphere. Before CV measurement, the nonaqueous electrolyte was prepared by the following procedure. Firstly, 0.01 mol redox compound (biphenyl, BP; or octafluoronaphthalene, OFN), 0.01 mol supporting electrolyte (tetrabutyl ammonium, Bu_4NClO_4), and 2.5 g alumina power (desiccant) were added into the flask, then the flask was repeatedly charged with nitrogen and degassed for three times; and at last, a 10 mL anhydrous organic solvent (N,N-dimethylformamide, DMF, for BP; or propylene carbonate, PC, for OFN) was injected into the flask to dissolve the redox compound and supporting electrolyte. A micro-platinum disk electrode (0.2 mm in diameter) was used as working electrode, and a platinum wire (0.5 mm in diameter) and a silver wire (1 mm in diameter) were used as counter electrode and reference electrode, respectively. CV test was carried out by a Solartron Analytical 1287 Electrochemical Interface coupled with a Solartron 1260A Impedance/Gain-Phase Analyzer. The cell resistance was measured by AC impedance method and all CV curves were IR-corrected.

1.2. Measurement of diffusion coefficient (*D*)

The diffusion coefficient of BP in DMF was obtained by using the Randles-Sevcik equation for reversible systems.[1] Specially, the relationship between the cathodic peak current density, $i_{p,c}$, and the diffusion coefficient of BP, D_O, is as follows:

$$i_{p,c} = (2.69\times10^5)n^{3/2}\cdot D_O^{1/2}\cdot C_O^*\cdot v^{1/2} \qquad \textbf{Eq. S1}$$

where, $i_{p,c}$ is the cathodic peak current density in A cm^{-2}, D_O is the diffusion coefficient of oxidative specie (BP) in cm^2 s^{-1}, C_O^* is the bulk concentration of oxidative specie (BP) in mol cm^{-3}, v is scan rate in V s^{-1}.

Similarly, the diffusion coefficient of ONF in PC was obtained. Specially, the relationship between the anodic peak current density, $i_{p,a}$, and the diffusion coefficient of OFN, D_R, is as follows:

$$i_{p,a} = (2.69\times10^5)n^{3/2}\cdot D_R^{1/2}\cdot C_R^*\cdot v^{1/2} \qquad \textbf{Eq. S2}$$

where, $i_{p,a}$ is the anodic peak current density in A cm^{-2}, D_R is the diffusion coefficient of reductive specie (OFN) in cm^2 s^{-1}, C_R^* is the bulk concentration of reductive specie (OFN) in mol cm^{-3}, v is scan rate in V s^{-1}.

1.3. Estimate of standard rate constant (k_0)

The standard rate constant, k_0, was obtained by using the Nicolson method.[2] For a cathodic CV process (like the CV of BP), the relationship between the standard rate constant and the Nicolson dimensionless number (Ψ) is given by the **Eq. S3**:

$$k_0 = [\frac{(\pi \cdot D_O \cdot f \cdot v)^{1/2}}{(D_O / D_R)^{\alpha/2}}] \cdot \psi \qquad \textbf{Eq. S3}$$

where, k_0 is the standard rate constant in cm s^{-1}; π is the mathematical constant; Ψ is the Nicolson dimensionless number, which is a function of the peak potential separation (ΔE_p) from CV curve. Note that the value of Ψ is obtained from the **Figure 3** in the Nicolson's classic paper;[2] D_O is the diffusion coefficient of oxidative specie (e.g., BP) and D_R is the diffusion coefficient of reductive specie (e.g., BP•$^-$), both in cm^2 s^{-1}; and v is scan rate in V s^{-1}; α is the charge transfer coefficient, dimensionless; and $f = (n \cdot F)/(R \cdot T)$, in which n is the number of electrons transferred in redox reaction, F is the Faraday constant (96485 C mol^{-1}), R is the ideal gas constant (8.314 J mol K^{-1}), T is the absolute temperature in K.

Note that the measurement of the diffusion coefficient of BP•$^-$ is rather complicated, and it is beyond the scope of this work. Well, it can be assumed that the diffusion coefficient of BP•$^-$ is reasonably close to that of BP, since they have the same molecular weight. Then the **Eq. S3** can be further simplified as follows:

$$k_0 = (\pi \cdot D_O \cdot f \cdot v)^{1/2} \cdot \psi \qquad \textbf{Eq. S4}$$

where, k_0 is the standard rate constant in cm s^{-1}; π is the mathematical constant; D_O is the diffusion coefficient of BP; v is scan rate in V s^{-1}; $f = (n \cdot F)/(R \cdot T)$; and Ψ is the Nicolson dimensionless number.

The k_0 results of the BP/BP•$^-$ redox pair are listed in the **Table S1**.

For an anodic CV process (like the CV of OFN), the relationship between the standard rate constant and the Nicolson dimensionless number (Ψ) is given by the **Eq. S5**:

$$k_0 = [\frac{(\pi \cdot D_R \cdot f \cdot v)^{1/2}}{(D_R / D_O)^{\alpha/2}}] \cdot \psi \qquad \textbf{Eq. S5}$$

where, k_0 is the standard rate constant in cm s^{-1}; π is the mathematical constant; Ψ is the Nicolson dimensionless number; D_R is the diffusion coefficient of reductive specie (e.g., OFN) and D_O is the diffusion coefficient of oxidative specie (e.g., OFN•$^+$), both in cm^2 s^{-1}; and v is scan rate in V s^{-1}; α is the charge transfer coefficient, dimensionless; and $f = (n \cdot F)/(R \cdot T)$, in which n is the number of electrons transferred in redox reaction, F is the Faraday constant (96485 C mol^{-1}), R is the ideal gas constant (8.314 J mol K^{-1}), T is the absolute temperature in K.

Similarly, by assuming the diffusion coefficient of OFN•$^+$ is reasonably close to that of OFN, the **Eq. S5** can be simplified as follows:

$$k_0 = (\pi \cdot D_R \cdot f \cdot v)^{1/2} \cdot \psi \qquad \textbf{Eq. S6}$$

where, k_0 is the standard rate constant in cm s^{-1}; π is the mathematical constant; D_R is the diffusion coefficient of OFN; v is scan rate in V s^{-1}; $f = (n \cdot F)/(R \cdot T)$; and Ψ is the Nicolson dimensionless number.

The k_0 results of the OFN•$^+$/OFN redox pair are listed in the **Table S2**.

2. Tables

Table S1. Calculation of k_0 for the BP/BP•$^-$ redox pair

v[a] (mV s^{-1})	ΔE_p[b] (mV)	Ψ[c] (dimensionless)	k_0[d] ($\times 10^{-3}$ cm s^{-1})	Average k_0 (cm s^{-1})	Standard deviation (cm s^{-1})
25	90	0.809	4.71	4.8×10^{-3}	0.4×10^{-3}
36	94	0.711	4.97		
49	96	0.665	5.43		
64	108	0.473	4.41		
81	114	0.421	4.41		
100	115	0.405	4.72		

[a] v: scan rate.
[b] ΔE_p: peak potential separation in CV curve.
[c] Ψ: Nicholson dimensionless number. The value was obtained from the **Figure 3** in the Nicolson's classic paper.[2]
[d] k_0: standard rate constant of the BP/BP•$^-$ redox pair.

Table S2. Calculation of k_0 for the OFN•$^+$/OFN redox pair

v (mV s^{-1})	ΔE_p (mV)	Ψ (dimensionless)	k_0 ($\times 10^{-3}$ cm s^{-1})	Average k_0 (cm s^{-1})	Standard deviation (cm s^{-1})
400	98	0.632	0.97	1.7×10^{-3}	0.4×10^{-3}
900	98	0.628	1.44		
1600	99	0.622	1.90		
2,500	104	0.521	1.99		
3,000	108	0.476	1.99		
3,600	111	0.446	2.05		

[a] v: scan rate.
[b] ΔE_p: peak potential separation in CV curve.
[c] Ψ: Nicholson dimensionless number. The value was obtained from the **Figure 3** in the Nicolson's classic paper.[2]
[d] k_0: standard rate constant of the OFN•$^+$/OFN redox pair.

3. Figures

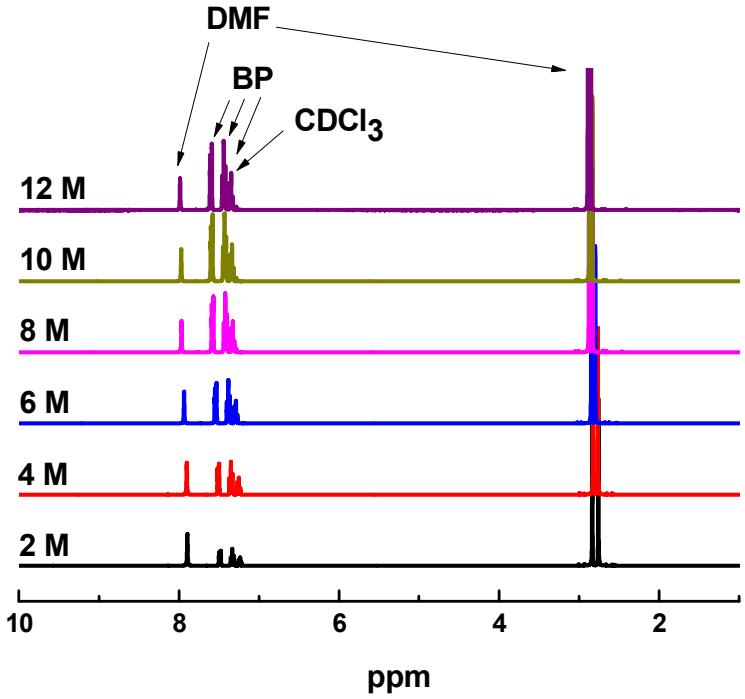

Figure S1. ^{1}H NMR spectra of BP solution in DMF with different apparent concentrations of added BP ($CDCl_3$ as NMR solvent). The detected BP concentration can be calculated by comparing the BP peak areas and DMF peak areas.

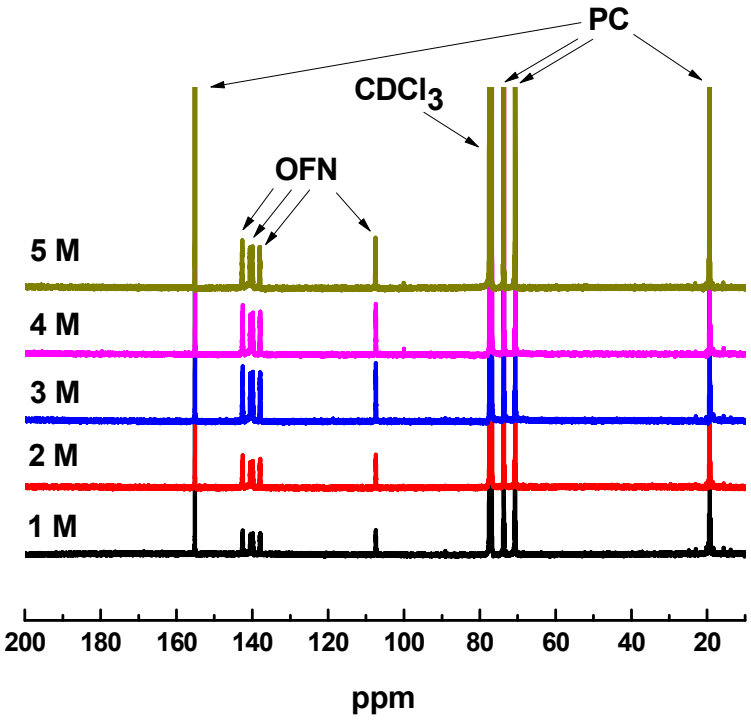

Figure S2. ^{13}C NMR spectra of OFN solution in PC with different apparent concentrations of added OFN ($CDCl_3$ as NMR solvent). The detected OFN concentration can be calculated by comparing the OFN peak areas and PC peak areas. Note: ^{1}H NMR spectroscopy is not appropriate for OFN, because the absence of protons in OFN molecule.

4. References

1. L. R. F. Allen J. Bard, *Electrochemical Methods: Fundamentals and Applications*, 2000.
2. R. S. Nicholson, *Anal. Chem.*, 1965, **37**, 1351-1355.